Damage Evaluation and Seismic Assessment of a Typical Historical Unreinforced Masonry Building in the Zagreb 2020 Earthquake: A Case Study—Part I

Uroš, Mario; Demšić, Marija; Šavor Novak, Marta; Atalić, Josip; Baniček, Maja; Jevtić Rundek, Romano; Duvnjak, Ivan; Košćak, Janko; Pilipović, Ante; Prevolnik, Snježan

Article

Damage Evaluation and Seismic Assessment of a Typical Historical Unreinforced Masonry Building in the Zagreb 2020 Earthquake: A Case Study—Part I

Mario Uroš [1,*], **Marija Demšić** [1], **Marta Šavor Novak** [1], **Josip Atalić** [1], **Maja Baniček** [1], **Romano Jevtić Rundek** [1], **Ivan Duvnjak** [1], **Janko Košćak** [1], **Ante Pilipović** [1] **and Snježan Prevolnik** [2]

[1] Faculty of Civil Engineering, University of Zagreb, 10000 Zagreb, Croatia; marija.demsic@grad.unizg.hr (M.D.); marta.savor.novak@grad.unizg.hr (M.Š.N.); josip.atalic@grad.unizg.hr (J.A.); maja.banicek@grad.unizg.hr (M.B.); romano.jevtic.rundek@grad.unizg.hr (R.J.R.); ivan.duvnjak@grad.unizg.hr (I.D.); janko.koscak@grad.unizg.hr (J.K.); ante.pilipovic@grad.unizg.hr (A.P.)

[2] Faculty of Science, University of Zagreb, 10000 Zagreb, Croatia; sprevolnik@gfz.hr

* Correspondence: mario.uros@grad.unizg.hr

Abstract: The city of Zagreb, the national capital and economic hub of Croatia, is situated in a seismically active region and hosts a significant array of historical buildings, from the medieval to Austro-Hungarian periods. These buildings possess varying but generally high degrees of vulnerability to seismic loading. This was highlighted in the Zagreb earthquake of 22 March 2020, emphasizing the need for seismic retrofitting in order to preserve this architectural heritage. In this paper, the seismic capacity of one such unreinforced masonry building is considered through a number of analysis methods, including response spectrum, pushover, and out-of-plane wall failure analyses. Given the advantages and disadvantages of the individual methods, their applicability and value in a seismic analysis is considered. Ambient vibration measurements before and after the Zagreb 2020 earthquake, used for model calibration, are also presented. Conclusions are drawn from each individual analysis and later compared. In conclusion, no single analysis method considers all relevant failure modes, and a combination of nonlinear static or dynamic analysis and out-of-plane analysis is recommended. Due to the large volume of the material, it is published in two parts, with ground motion record selection, dynamic analysis, and a comparison of the results published in part two.

Keywords: earthquakes in Croatia; unreinforced masonry building; seismic assessment; nonlinear static analysis

1. Introduction

Throughout history, the seismic vulnerability of unreinforced masonry (URM) buildings in Croatia has been quite high, as confirmed by many post-earthquake reports [1–3]. The main reason for this is the construction material, along with the lack of knowledge about seismic design available in the periods when this typology was predominantly built. It was common to consider only vertical loads. The earthquake on 22 March 2020 with a magnitude of 5.4 (Mw) hit the urban area of Zagreb, with the epicenter located about 7 kilometers northeast from the center of Zagreb at a depth of 10 kilometers [4,5], causing heavy damage to many traditional unreinforced masonry (URM) buildings in the historic center of Zagreb. The intensity at the epicenter was estimated at VII degrees on the MCS scale. Not long after that, on 29 December 2020, a strong earthquake of magnitude 6.4 (Mw) hit central Croatia with the epicenter 6 km southwest of the city of Petrinja, which is about 50 km from Zagreb (Figure 1). The intensity at the epicenter near Petrinja was estimated at VIII degrees on the MCS scale and, in Zagreb, the intensity was estimated at VII degrees on the MCS scale [6].
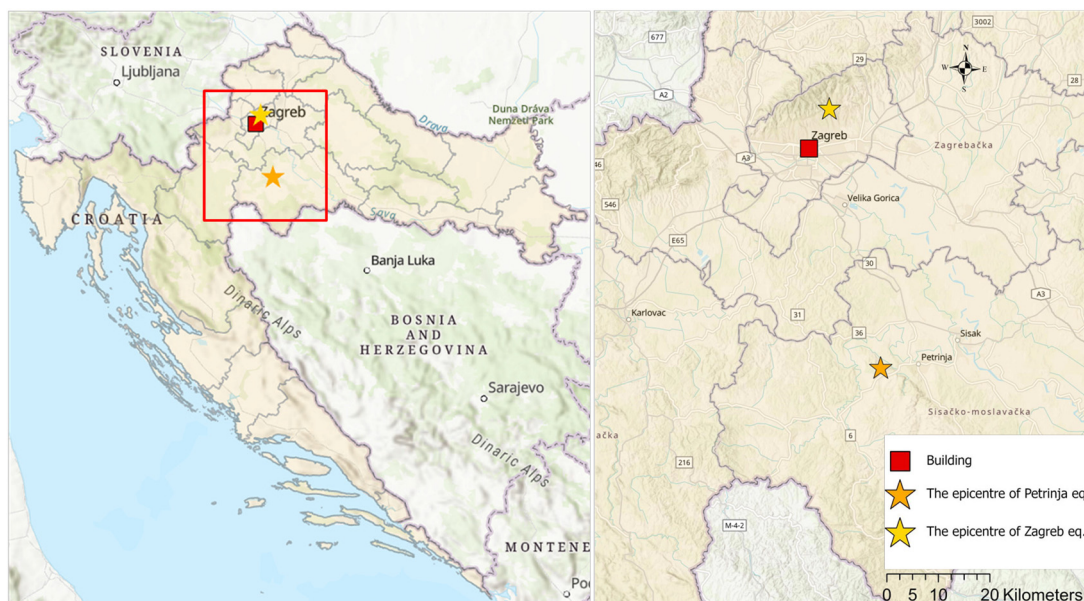
Figure 1. Geographical location of the Zagreb region with location of the building and the epicenters of the 2020 earthquakes.

This strong earthquake caused extensive damage to URM buildings, particularly in Sisak-Moslavina County, but also caused progressive damage to buildings in Zagreb [7].

The center of Zagreb has a very old building stock, with URM buildings that are more than three stories high and mainly built standalone or within row aggregates. The city center features an array of styles from the medieval to Austro-Hungarian periods (1867–1918), primarily composed of old unreinforced masonry structures, as classified in seismic risk assessment [8], which were built after the Zagreb earthquake in 1880 [9]. Their vulnerability was highlighted during the 2020 earthquakes, emphasizing the need for seismic retrofitting to preserve this architectural heritage [4,10].

The observed damage included collapsed and damaged chimneys, attics, gable walls, and various other inadequately supported elements (domes, etc.). Other typical damage included separation of gable walls along the height, roof damage, in-plane damage of masonry walls (visible diagonal cracks with cracks often following mortar joints), and damage to lintels and vaults, staircases, and partition walls. As such, the observed failure mechanisms included out-of-plane and in-plane wall failures. Many buildings were affected by the formation of diagonal cracks in load-bearing (structural) and more often non-bearing (non-structural) walls and lintels due to exceedance of the in-plane bearing capacity [1,11]. With regard to the safety of occupants, decorative elements such as roof domes, portals, cornices on facades, and decorative sculptures also suffered considerable damage, occasionally falling on to the roads and sidewalks. Usually, these elements were not properly restrained.

The classification and degree of damage caused by the earthquake and the building usability are described in detail in [12]. Most buildings that were built after 1964 did not suffer any significant damage. Only the infills and the connections with frame structure were occasionally damaged in reinforced concrete frames with infills.

The results obtained through on-site building-by-building inspection of usability, including both residential and commercial–residential buildings, are shown in Figure 2. It can be observed that most of the damage was concentrated in the historic center of the city.

| (**a**) | (**b**) |

Figure 2. Damage to residential and commercial–residential buildings on: (**a**) a perspective view of the city of Zagreb according to usability tags (colors) and gross floor areas of buildings (heights of columns) and (**b**) a perspective view of the historical center according to buildings' usability tags from the GIS-based Building Usability Database (source: Croatian Centre for Earthquake Engineering—CCEE).

Flexible wooden beam floors, poor brick and mortar quality, and inadequate connections between load-bearing walls and the floor structures are common for this typology. Also, a dominant direction of load-bearing walls parallel to the street can usually be noted, which supports wooden beams [11,13]. More recent studies that deal with the investigation of residential buildings in the city center of Zagreb can be found in [14–16].

Problems with conducting seismic assessment of URM buildings are pronounced and there are many studies and papers that have tried to solve them [17]. For instance, masonry is an inhomogeneous material and its properties depend on many factors that are often not known and are difficult to comprehensively take into account in analysis.

A numerical analysis of a typical URM building in Zagreb is given in [14], where the building is modeled as freestanding and in row aggregate. In the numerical investigations, the equivalent frame method is applied in the Tremuri software (research version), taking into account the in-plane response and performing nonlinear static and dynamic analyses using the Zagreb and Petrinja earthquake records.

The influence of the building aggregates in the center of Zagreb is very important. The buildings are built so that the gable walls touch each other. Information on the influence of a building aggregate on the fragility of the individual building can be found in [17,18], but it should be emphasized that very often this aggregate is interrupted. This is also the case with the typical building considered in this paper, which has no neighbors on one side.

In the unreinforced masonry (URM) building typology, there is a high seismic vulnerability to out-of-plane failure of walls, initiated by perpendicular seismic actions [19]. Factors such as poor connections of roof and floor structures, lack of horizontal and vertical constraining elements, and relatively low vertical loading on top floors contribute significantly to the development of a kinematic mechanism. The effect of such construction was observed in the Zagreb 2020 earthquake, where predominant damage was caused by overturning of gable walls, chimneys, and building ornaments. To a lesser degree, larger out-of-plane mechanisms were observed, while in-plane failure mechanisms were predominantly observed on partition walls [4].

Different approaches to seismic assessment of masonry, as well as different strategies of analysis, have been proposed in [20], with a comprehensive review of the existing modeling strategies for masonry structures.

Moreover, ref. [21] gives a comparison of different methods of analysis and different numerical models to estimate the seismic behavior of unreinforced masonry buildings with flexible diaphragms, while [22] presents the comparison of the results of nonlinear static analyses carried out using six software packages on a numerical model of a masonry building.

In [23], the authors provide a comprehensive review of the critical aspects of nonlinear modeling for evaluating the seismic response of masonry structures where the principles of numerical modeling of masonry buildings are given. Furthermore, ref. [24] gives a critical analysis and systematic comparison of the results on URM buildings obtained by using several modeling approaches and software package tools on benchmark examples.

Existing irregular masonry buildings are investigated by means of the equivalent frame modeling technique and nonlinear static analysis in [25], giving particular attention to the selection of load patterns in pushover analysis, and the results are compared with the results of nonlinear dynamic analyses.

A newly developed microelement for a frame element modeling approach that accounts for both in-plane and out-of-plane failure modes is used in research study [26] for modeling historical masonry buildings with timber floors, and it is highlighted that modeling the out-of-plane behavior has a significant impact on the seismic fragility curves. Furthermore, fragility curves for typical URM buildings with the out-of-plane effect are developed and given in [27,28].

For URM buildings, the systematic analysis of seismic behavior must also include the assessment of out-of-plane wall failure [29,30], a form of failure that involves an interaction of many mechanisms and is currently the focus of research studies. A still limited number of experimental research campaigns focus on clarifying some issues related to out-of-plane behavior, such as the identification of appropriate boundary conditions [31], the influence of wall morphology [32], the loading and displacement capacity of the mechanism [33–36], etc. In addition, out-of-plane behavior research is further developed through numerical analyses, including the development of NURBS-based software to compute local mechanisms [37], a multi-level procedure to identify the geometry and load multiplier of a rigid-body failure mechanism [38], and more detailed numerical models using the Lattice Discrete Particle Model to capture damage evolution and fracture propagation, i.e., local mechanism formation [39].

The problem of torsional effects in irregular masonry buildings is presented in [40] due to nonlinear static analyses and using different modeling approaches. Validation of simplified approaches is generally provided with reference to regular structures, and the conclusion is that structural irregularities are important to consider and can be taken into account through a simplified approach.

Modeling of masonry, even with many material parameters measured on-site, is a relatively demanding task. The problem is compounded by quality measurements of material properties being relatively complex, destructive, and expensive, requiring relatively large portions of walls, and still leaving relatively high uncertainty. When observing numerical models, problems that stand out are interactions between different failure modes (in and out of plane), inadequate connections between perpendicular walls that considerably contribute to out-of-plane failures, and the identification of local failure mechanisms of individual elements [29]. Another problem is the modeling of construction details, such as overhangs, vaults, the use of jack arches, the connection between wooden floors and URM walls, etc.

Furthermore, creating a model that will take into account all relevant failure mechanisms with sufficient accuracy is challenging just from a numerical perspective, so simplifications are used and various approaches are considered in different software packages. In order to encompass all significant modes of failure, the numerical model needs to be complex. However, increasing complexity also increases the need for input parameters, which are, as already mentioned, scarce [23].

Against that background, the objective of this study was to conduct a detailed seismic assessment of a typical URM building. This was achieved by applying different modeling methods to predict relevant failure modes and the seismic capacity of the damaged URM building. Valuable results were obtained through on-site building testing comprising dynamic parameters before and after the 2020 Zagreb earthquake. Due to the volume of the work carried out in this study, it has been divided into two papers, where the first

one (this article) focuses on building description, parameters considered in modeling, and a number of analysis and modeling methods. The following analysis methods are considered: linear elastic response spectrum and static pushover analysis to account for the global building response, and kinematic analysis of the most common mechanisms for the local out-of-plane response. The second paper describes damage caused by the Zagreb 2020 earthquake and the measured parameters of the damaged building, as well as gives the results of a dynamic analysis of the building response. When assessing the applicability of the results from different models, it is important to emphasize that simpler modeling methods, which are intended to be conservative, will not always consider all possible failure modes and, therefore, may not be conservative or even safe to apply. For URM buildings with timber floors, a dominant failure mechanism not considered by many simpler modeling techniques is out-of-plane failure [19]. Therefore, in settings such as Zagreb, when considering the load capacity of a building, techniques are required that take into account all significant modes of failure of the building, and in doing so, adequately assess its seismic performance.

2. As-Built State of the Case Study Building and Seismic Hazard at the Site

The entire historical part of the Lower Town of Zagreb was built in the same style, which was based on the guidelines of Austro-Hungarian construction techniques. The buildings mainly have three load-bearing walls parallel to the street, on which a wooden floor structure rests. These walls decrease in thickness with height. The gable walls are perpendicular to the street and they are not load-bearing walls so they are relatively thin. The typical building is often divided into two units, the street part and the courtyard part, and they are connected by a staircase. Structurally, there is a problem of discontinuity of the building. All floor structures comprise wooden beams except for the basement, where there is usually a Prussian vault. The buildings usually have four to five floors above the ground.

The building analyzed in this study was built in 1922 and is a typical example of a building type found in the Lower Town of Zagreb [1,5] (Figure 3). The epicentral distance to the analyzed building is approximately 8 km.
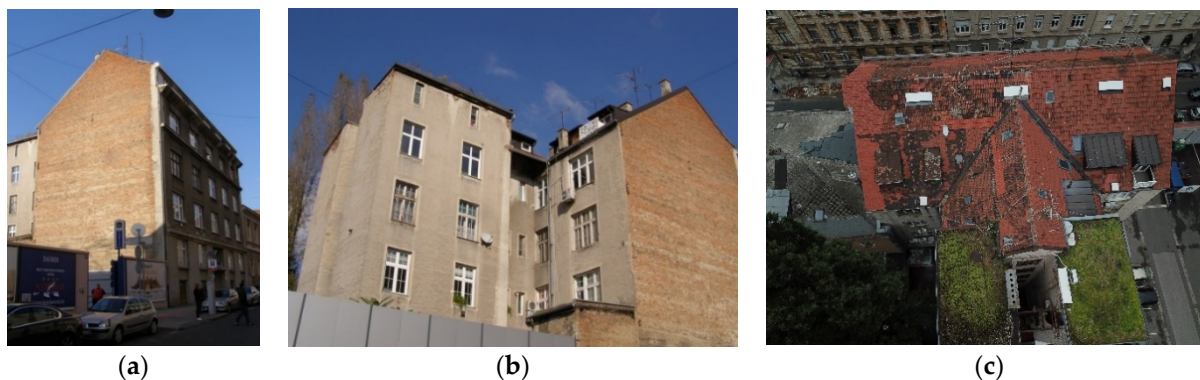

(a)   (b)   (c)

Figure 3. Photographs of the case study building: (**a**) south- and street-facing facade; (**b**) side view; (**c**) aerial view.

The dimensions of the floor plan are 24.4 × 12 m on the street side and 10.6 × 12 m on the courtyard side, resulting in a gross floor plan area of approximately 407 m^2 and total gross area of the building of around 2440 m^2. The building consists of a basement, ground floor, three stories, and an attic (Figure 4). The basement has a height of 3 m, while the ground and first floors are 3.5 m high. The total height of the building is 22.70 m. The annexes on the courtyard side of the existing building are connected to its main part, which faces the street. The floor plan of the building is relatively irregular, with heterogeneous floor structures.
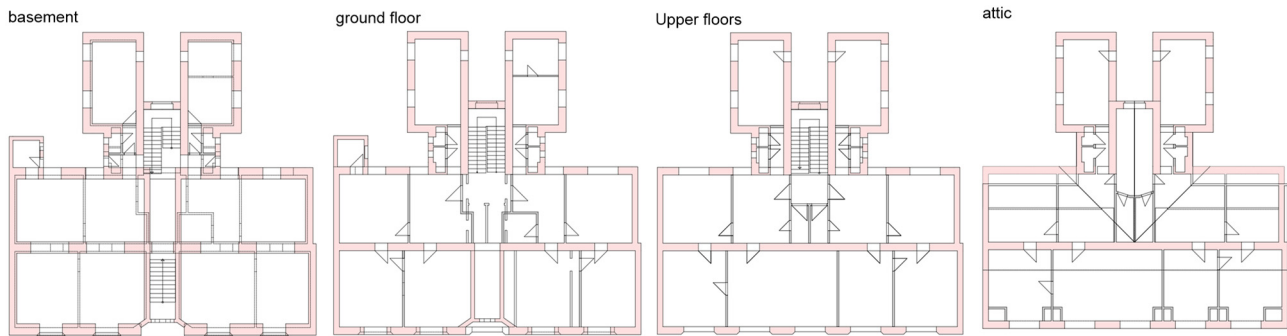
Figure 4. Floor plans of the as-built state of the building.

The structure consists of a system of interconnected solid brick walls that extend continuously from the foundation to the roof, so the criterion of regularity in elevation is met. The load-bearing walls are 90, 60, 45, 30, and 15 cm thick, constructed of old solid clay brick (290 × 140 × 65 mm). The partition walls are 7 and 15 cm thick, also built of solid bricks. The walls are connected by spandrels, parapets, and reinforced concrete (RC) beams. The foundations consist of 90 cm thick brick walls built over a layer of concrete.

The floor structure (Figure 5) located above the basement on the street side of the building is a solid RC slab with a system of RC beams. As for the upper floors, they feature timber joists that are arranged in a transverse manner, with rubble filling used in the floor structure. During renovations, RC slabs measuring 8 cm in thickness were added above the ground floor and the third floor on the southern side of the building. The floor structure consists of timber joists with a layer of concrete with unknown reinforcement and properties on top. In the middle part of the building next to the staircase landing, there is an RC slab supported by RC beams on the edge.
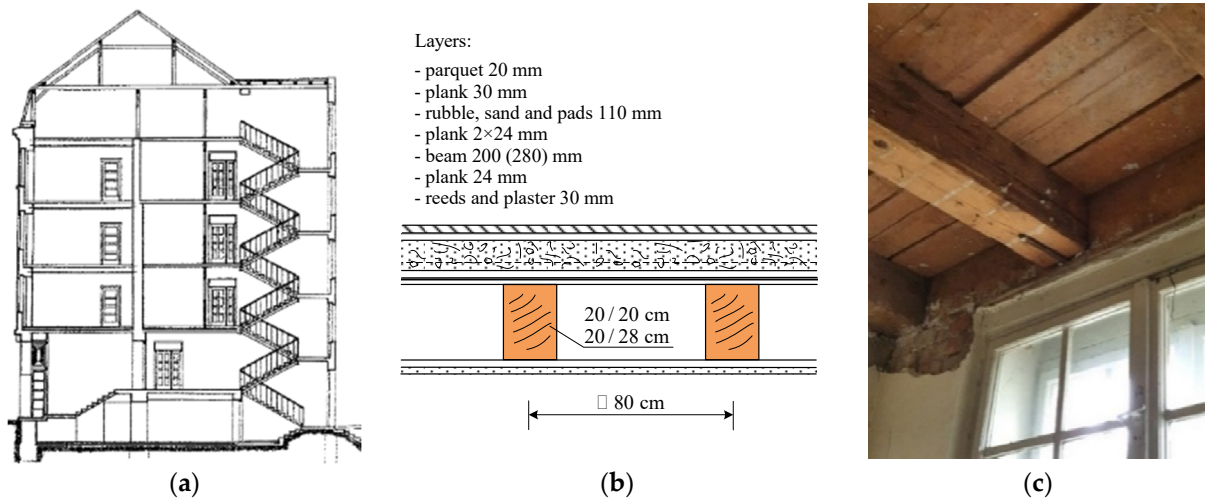

Layers:

- parquet 20 mm
- plank 30 mm
- rubble, sand and pads 110 mm
- plank 2×24 mm
- beam 200 (280) mm
- plank 24 mm
- reeds and plaster 30 mm

20 / 20 cm
20 / 28 cm

⌀ 80 cm

(**a**) (**b**) (**c**)

Figure 5. Cross-section and timber floor structure. (**a**) cross-section of the building; (**b**) layers of the timber floor structure; (**c**) photograph of the timber floor structure.

The roof structure is made of timber, and the attic has been adapted into a living space over time. Inside the building, there is a double staircase made of prefabricated RC elements, which are supported by walls and steel profiles. Additionally, there are RC platforms incorporated into the staircase design.

The first inspection of the building was carried out on the day of the earthquake, 22 March 2020, and the building was categorized as temporarily unusable. Severe damage to partition walls, and moderate damage to most load-bearing walls except for the courtyard wall that was severely damaged, was observed. The gables in the attic space of the building and the chimneys were also severely damaged. Slight damage was recorded to the floor

structures, the staircase, and the roof structure, with indications of very severe damage to the chimney and some of the tiles falling off. Photographs of the damage are shown in Figure 6.

Figure 6. Photographs from damage assessment of the building after the Zagreb earthquake.

The seismic loading was determined on the basis of a reference peak ground acceleration (PGA) for the earthquake return periods of 95, 225, and 475 years. The seismic hazard map of the Republic of Croatia [41], which can be accessed online at http://seizkarta.gfz.hr/hazmap/ (accessed on 5 May 2023), was used for the calculation.

3. Preliminary Assessment of the Building's Vulnerability

A preliminary assessment of the building's vulnerability was conducted using a macroseismic method, in accordance with the RISK-UE project [42], with building vulnerability expressed through a vulnerability index [43]. Roughly, the solution is the mean damage grade, governed by the expression (1):

$$\mu_D = 2.5 \left[1 + tanh \left(\frac{I + 6.25V - 13.1}{Q} \right) \right] \tag{1}$$

where V is a vulnerability index describing the building type and building properties governed by the expression (2):

$$V_I^z = V_I^c + \Delta V_m + \Delta V_R \tag{2}$$

$$\Delta V_m = \sum_{j=1}^n V_{m,j} \tag{3}$$

In the equation, V_I^c is the most probable value of the vulnerability index depending on the building type, ΔV_m is a behavior modifier based on building properties (such as height, soft story, etc.), and ΔV_R is a regional vulnerability factor that accounts for the particular quality of certain building types based on expert judgment.

The mean damage grade is calculated for the EMS-98 macroseismic intensities 8 and 9 [44], which is in line with the seismic hazard in the city of Zagreb. The obtained values (Table 1) show that for both macroseismic intensities, very heavy damage can be expected.

Table 1. A preliminary assessment of the building's vulnerability.

Average story height [cm]	330
Ground floor level relative to actual ground [cm]	120
Total height (ground to rooftop) [m]	22.7
Number of stories	5
Material used for load-bearing structure	Masonry (full brick with lime mortar)
Technology of construction	In situ
Load-bearing system	Wall system
Presence of tie-columns	No
Presence of tie-beams	No
Foundation type	Strip foundations—unconnected
Foundation material	Masonry
Foundations at different levels	No
Material of floor structure	Wood
Type of floor structure	Wooden beams with a heavy soft plate (gravel and wood planks, etc.)
Material of roof structure	Wood
Roof shape	Gable roof
Position in aggregate	At the end of a row
Interaction with adjacent building	Next to a lower building
Floor levels relative to the adjacent building	Irregular
Floorplan shape	Irregular
Structural regularity in elevation	No irregularities
Soft story	No
Regularity in plan	Torsional eccentricity
Year of reconstruction	0
Reconstruction	Negligible
Added stories	Yes
Total ground floor area [m^2]	380
Total floorplan area of the building [m^2]	1900
Ground floor wall area in X direction [m^2]	23.82
Ground floor wall area in Y direction [m^2]	30.36
Ground floor wall area percentage in X direction	6
Ground floor wall area percentage in Y direction	8
ag475 [g]	0.25
ag95 [g]	0.13
Total building weight [kN]—without basement	31,608
Behavior factor q	1.5
Soil category according to EC8	C
Estimated first period T1 [s]	0.362

Table 1. *Cont.*

Response spectrum ordinate for T1—A(T1) [g]	0.498
Lateral force Fb [kN]	10,654
Lateral force coefficient—BS [-]	0.337
Average shear stress τ_X [MPa]	0.447
Average shear stress τ_Y [MPa]	0.351
Building type (RISK UE)	M31H
$V_I{}^c$	0.74
Maintenance	−0.04
Number of stories	0.06
Structural system	0.02
Soft story	0
Floorplan irregularities	0.04
Irregularities in height	0
Added stories	0.04
Roof (heavy roof with thrust)	0.04
Reconstruction	0
Position in aggregate	0.06
Buildings of different heights in the aggregate	0.02
Staggered floors of buildings in the aggregate	0.02
Foundations	0
Terrain morphology	0
V_R	0
$V_I{}^z$	1.00
μ_D(VIII)	3.58
μ_D(IX)	4.24

4. Experimental Measurements

4.1. Mechanical Properties

In order to determine the mechanical properties of masonry, suitable experimental methods were selected by referring to proven research work. The first method was based on the determination (in situ) of the shear of the mortar in the masonry without determining the vertical compressive stress, while the second was based on the determination of the compressive strength of solid bricks in the laboratory.

The location of the in situ shear tests was chosen in accordance with the recommendations of the Eurocode (HRN EN 1998-3 [45], Table 3.1), with the aim of achieving the coefficient of knowledge of the material CF_{KL3} = 1. In general, this is often not possible due to the availability of the position/location during the investigation, so the number and position are often chosen based on previous experience. The purpose of the selected in situ test is to determine the shear strength between two horizontal bed joints bounding a single brick unit. This method is a modification of the well-known "shove test", which takes into account the control of vertical stress in accordance with the procedure and the ASTM C1531-16 standard [46]. Taking into account the linear regression, it is possible to determine the shear strength without the normal compressive stress (f_{v0}) according to Coulomb's law

$$f_{v0} = f_v - \mu\sigma_0 \tag{4}$$

$$f_v = \frac{F_h}{A_u + A_I} \tag{5}$$

where f_v is the shear strength of the masonry, μ is the coefficient of friction, σ_0 is the normal compressive strength, F_h is the experimentally determined shear force at the time of shear failure, and A_u and A_l are the upper and lower areas of the brick. With the selected in situ method, it is possible to obtain f_{v0}. First, f_v must be determined experimentally, and then the value of the friction coefficient can be assumed to be 0.4 (HRN EN 1998-3) and the vertical compressive stress can be obtained from the numerical model. The advantage of the chosen method is that it can be carried out in a short time (45 min/location). However, the disadvantage of the method lies in the assumptions already mentioned. In this study, the protective layer of the plaster was removed at a total of eleven locations, a shear test was performed at seven locations, and the remaining four locations were only used for visual identification of the masonry. All shear tests were carried out approximately 100 centimeters above the floor, on the locations shown in Figure 7. The results of the shear test and compressive strength we performed are summarized in Table 2.
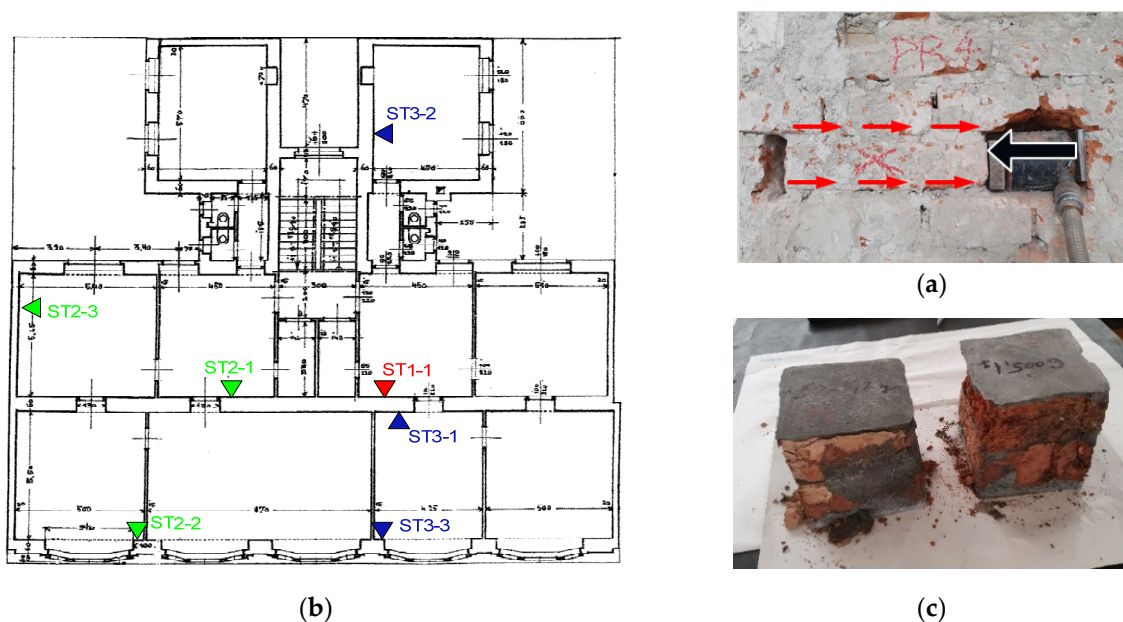

Figure 7. (**a**) Characteristic floor plan and locations of the shear test, (**b**) shear test of mortar without control of vertical stress, (**c**) samples for determination of compressive strengths of solid bricks.

Table 2. Results of experimental testing of shear strength and compressive strength of solid brick.

Floor Location	Label	Notes	Shear Strength f_v [MPa]	Compressive Strength [MPa]
First floor	ST 1-1	CLBW	0.577	7.71
Second floor	ST 2-1	ELBW	0.593	6.84
	ST 2-2	CLBW	0.500	-
	ST 2-3	EGW	0.259	-
Third floor	ST 3-1	CLBW	0.304	-
	ST 3-2	ELBW	0.389	-
	ST 3-3	ELBW	0.333	-

Abbreviation: CLBW central load-bearing wall, ELBW external load-bearing wall, EGW external gable wall.

If the result of the shear strength ST2-3 disregarded (as the test was carried out on a non-load-bearing wall), then average values can be obtained depending on the floor plan, which decrease with the self-weight of the structure. In the laboratory, an average

compressive strength of 7.28 MPa and a specific weight of 1843 kN/m^3 were determined on two extracted solid brick samples.

4.2. Determination of the Structural Modal Parameters

The dynamic parameters are certainly among the most important data for the calibration of the initial numerical model. The structural dynamic properties were determined based on operational modal analysis (OMA) by using a piezoelectric accelerometer (PCB Piezotronics, type 393B31) with the nominal sensitivity of 10 V/g (PCB Piezotronics, Depew, NY, USA), an analyzer (Brüell&Kjaer, type 3560C, Brüell&Kjaer, Naerum, Denmark), and the accompanying software. Since the estimation is performed for ambient vibrations, the stiffnesses of the load-bearing elements have tangential values and are determined with a vertical load. Dynamic parameters are also important for monitoring the condition of a building: if the building parameters are known to be intact, changes in these parameters can be used as an indicator of changes in the structural integrity of the building (e.g., due to reconstruction or structural damage caused by earthquakes and/or natural material degradation).

The measurement of the ambient vibrations of the studied building was carried out in October 2014 and September 2020 (number of degrees of freedom measured: 44). The measurement points were located in the core of the staircase and are shown in Figure 8. The measurements were performed in two horizontal directions (X and Y directions). A classical frequency domain decomposition (FDD) was used for the estimation of natural frequencies (Table 3) and mode shapes (Figure 8), while the enhanced frequency domain composition (EFDD) method was used for the estimation of damping.
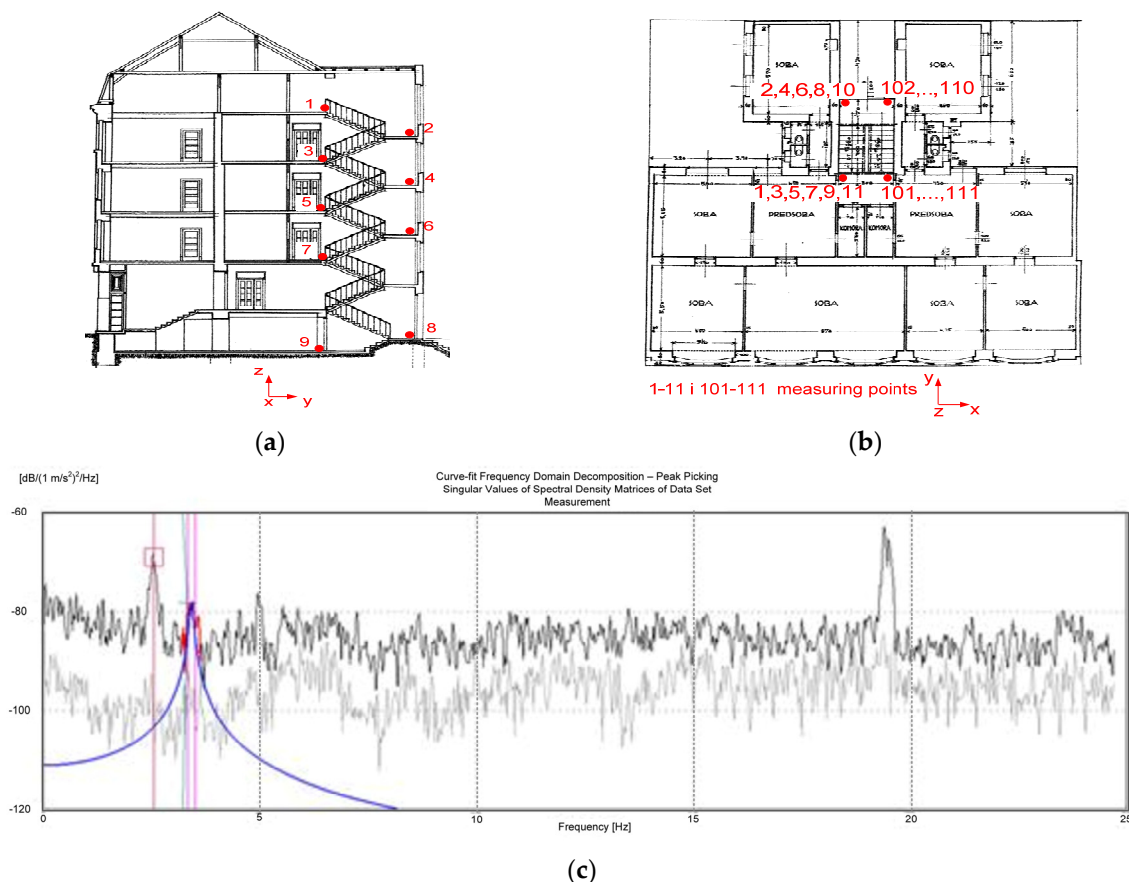

Figure 8. Measurement point locations (**a**) in cross-section and (**b**) in floor plan. (**c**) Characteristic record of frequency domain decomposition (FDD) for the determination of natural frequencies.

Table 3. Experimental values of natural frequencies and relative damping.

Natural Frequency ± St.dev (Hz)		Relative Damping ± St.dev (%)	
October 2014	**September 2020**	**October 2014**	**September 2020**
2.55 ± 0.02	1.98 ± 0.02	1.46 ± 1.02	2.87 ± 0.80
3.10 ± 0.03	2.63 ± 0.02	2.84 ± 1.75	2.76 ± 1.19

Figure 9 graphically shows the main vibration modes of the building and allows for a comparison of the measurements taken before and after the earthquake in Zagreb. It may be noted that the mode shapes do not change between the two measurement periods (before and after the earthquake). It is obvious that the periods of the fundamental modes of vibration were prolonged due to the damage caused by the earthquake. For example, the first mode of vibration in the X direction (longitudinal direction) was 0.39 s before the earthquake but 0.50 s after the earthquake. This corresponds to a reduction in global stiffness of about 40%. The second mode of vibration, which predominates in the Y direction (transverse direction), had a period of 0.32 s and 0.38 s after the earthquake. Thus, the reduction in global stiffness due to the earthquake damage is about 30%. These data clearly show that the stiffness of the load-bearing elements of the building has decreased.

2.55 Hz (0.38 s) (2014) vs. 1.98 Hz (0.50 s) (2020)   3.10 Hz (0.32 s) (2014) vs. 2.63 Hz (0.38 s) (2020)
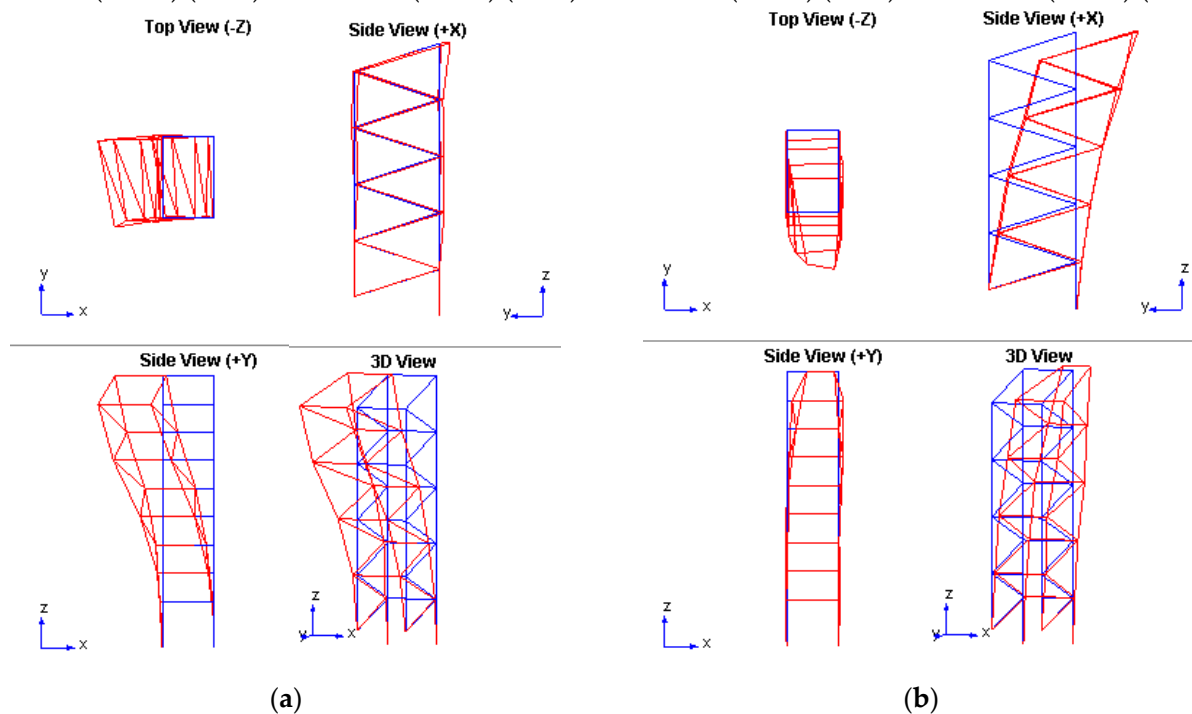

(**a**)   (**b**)

Figure 9. Experimentally obtained (**a**) first (dominant) translation mode shape in y direction, and (**b**) second translation mode shape in X direction. The blue lines represent the undeformed shape, while the red lines represent the deformed shape.

5. Numerical Models and Analysis Methods

5.1. Model Description

Various numerical models were generated using the software ETABS v.17 [47] through the implementation of the finite element method. A three-dimensional representation of the numerical model that shows a vertical and horizontal load-bearing system is shown in Figure 10a, and a more detail plan layout for each story and values of the available shear areas of load-bearing walls are displayed in Figure 10b,c. Material parameter values were determined through experiments. After processing the results and comparing them with

the prescribed values, the values shown in Table 4 were adopted. It is worth noting that some minor interventions in walls and lintels were made in low-quality concrete (C12/15). The partial factor for the material property was taken to have a value of 1.5 for linear calculations, while for nonlinear calculations, the value was 1.0.
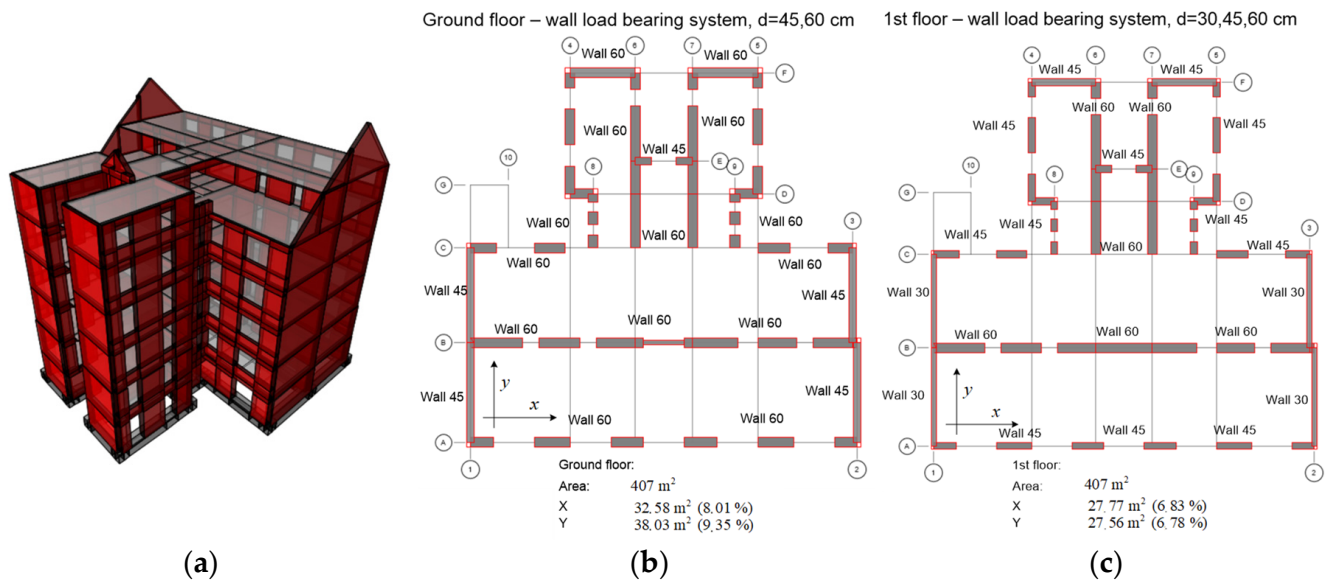

(a)   (b)   (c)

Figure 10. Numerical model of a building created in ETABS v.17. Vertical load-bearing system of masonry walls with dimensions by floors. (**a**) 3d numerical model; (**b**) layout of the walls on the ground floor; (**c**) layout of the walls in the first floor.

Table 4. Mechanical properties of the masonry.

	Compressive Strength	Initial Shear Strength	Young's Modulus	Shear Modulus	Specific Weight	Tension Strength
Masonry typology	f_m [MPa]	f_{vm0} [MPa]	E [MPa]	G [MPa]	γ [kN/m^3]	f_t
Masonry in bricks and lime mortar	3.4	0.16	1500	500	18	0.114

The model incorporated the cracking of the cross-sections based on Croatian standards HRN EN 1998-1 and HRN EN 1998-3 (adopted Eurocode 1998 Standard). The initial flexural stiffness of RC beams, columns, and walls was reduced to 50%. Similarly, the shear stiffness of all elements was considered to be 50% of the initial stiffness. The nonlinear behavior of the load-bearing elements accounted for local formation of plastic hinges. The analysis initially focused on the bearing capacity of walls and spandrels, considering various failure mechanisms. It was found that shear failure induced by diagonal cracking or sliding was the dominant mode of failure. The confidence factor in this study was taken as 1.00.

The nonlinear behavior of the model and the elements was taken into account through concentrated plastic hinges placed at critical points in the structure. Concentrated plasticity is defined in frame elements but also in shell elements, and the latter was the most important here because of the walls. The load capacity of walls and spandrels was determined based on various failure mechanisms. To determine the capacity curve of a load-bearing wall, all failure mechanisms were observed and the predominant one was selected (Table 5). It was found that shear failure arising from the development of diagonal cracks in the wall or shear failure from the sliding of the wall was dominant. There was also a failure of the wall that arose due to crushing of the material in the toe of the wall, which was initiated by its

rocking. The deformation capacity and plastic hinge curves of masonry walls and lintels were defined in accordance with HRN EN 1998-3. The load-bearing capacity of reinforced concrete beams was calculated by accounting for and critically analyzing various standards such as HRN EN 1998-3 and ASCE/SEI 41-13 [48].

Table 5. Wall-bearing capacity criteria and mechanical parameters.

In-Plane Failure Mechanisms	Analytic Expression
Crushing/bending	$V_{\text{Rd,r}} = \psi \frac{\sigma_0 t_w l_w^2}{2h} \left(1 - \frac{\sigma_0}{f_{\text{Mc}}}\right)$
Shear diagonal cracking	$V_{\text{Rd,t}} = l_w t_w \frac{f_{\text{Mt}}}{b} \sqrt{\left(1 + \frac{\sigma_0}{f_{\text{Mt}}}\right)}$
Shear sliding	$V_{\text{Rd,ts}} = l_{wc} t_w (f_{v0} + \mu \sigma_d)$

f_{Mc}—masonry compressive strength; f_{Mt}—diagonal tensile strength of masonry; f_{v0}—initial shear strength of masonry; μ—friction coefficient; t_w—pier thickness; l_w—pier length; l_{wc}—length of compressed section; h—pier height; σ_0—normal compressive stress of pier; σ_d—average vertical stresses in the compressed section of the pier; ψ—correction factor for constraints (1.0 for cantilever and 2.0 for beam fixed on both ends); b—correction coefficient depending on stress distribution of the section (usually equals h_w/l_w, but no more than 1.5 and less than 1.0, where h_w is the height of the panel).

The analysis utilized the assumption of semi-rigid diaphragms for the model. Nevertheless, it was crucial to ensure this property of the building in order to effectively utilize the in-plane bearing capacity of the walls. A separate analysis was later carried out for out-of-plane failure mechanisms assuming a lack of quality connections between the walls and the floor structures.

The total load of the structure consisted of the masonry weight and the weight of the floor structures, which was approximately 2.5 kN/m^2 in all floor levels except for the basement, where it was 3.5 kN/m^2. The additional permanent load was taken to be 1.5 kN/m^2, and the imposed load was 2 kN/m^2. Finally, the total estimated mass of the building above the foundation was about 3222 t.

Limit states were adopted according to Croatian Technical Regulation for Building Structures (CTRBS), which was introduced after the earthquakes in Croatia in 2020, and established seismic safety requirements for retrofitting of the damaged buildings. Unlike HRN EN 1998-3, which defines three limit states (near collapse (NC), significant damage (SD), and damage limitation (DL)), the CTRBS only considers the limit state of significant damage (SD). Under this limit state, the safety factor can be reduced to 0.5 for level 2 and 0.75 for level 3 of retrofitting.

Level 2 is the mandatory minimum retrofit requirement for residential buildings, like the one examined in this study. It is approximately equivalent to an earthquake event with a return period of 95 years, specifically for the limit state of significant damage. However, it should be emphasized that retrofit level 2 does not provide a satisfactory level of safety.

5.2. Vertical Loading Analysis

The results for the vertical loads represent the initial state for the nonlinear analysis, either static or dynamic. This is due to the stress state of elements being directly corelated with their stiffness and ductility when loaded with a lateral load. For the masonry building considered in this study, the most significant influences were those of the axial force on the rotational and shear capacity of the walls. Only the most significant results are provided below, to facilitate an interpretation of the effects of seismic loading on the structure, due to the vast amount of data generated.

The subfigures in Figure 11 show the load-bearing elements' normal stresses due to the permanent vertical loads in the basement and on the ground floor. The average stresses of the walls are mainly between 0.3 and 0.6 MPa.
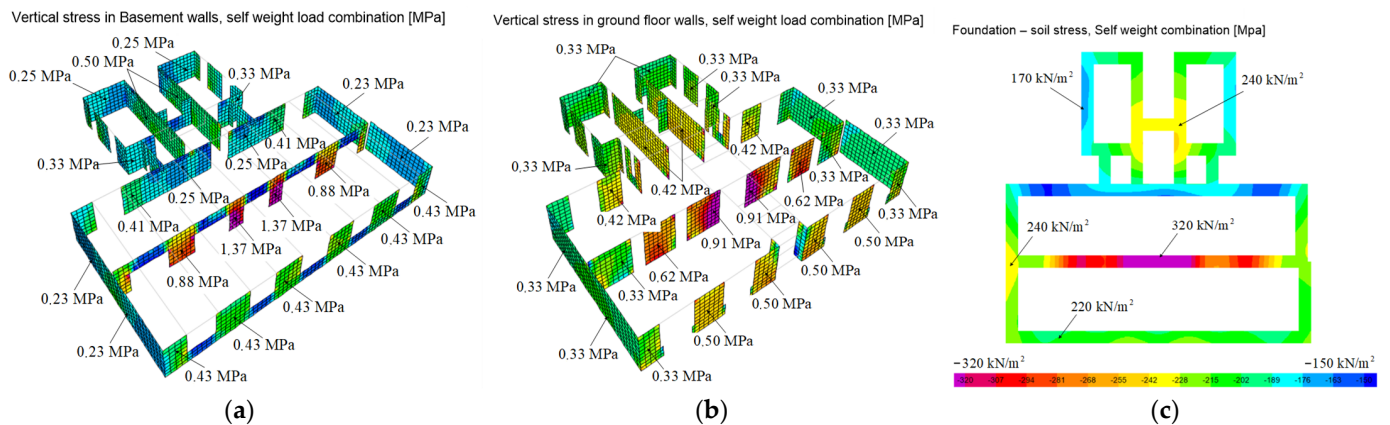
Figure 11. Normal stress distribution and soil stresses (for permanent vertical load). (**a**) stress distribution in the basement walls. (**b**) stress distribution in the ground floor walls. (**c**) soil stresses.

5.3. Dynamic Properties of the Building

Calibration of the numerical model was carried out to obtain the measured values from the ambient vibration measurements. To achieve this, the internal forces in the structure were analyzed and, based on them, the degree of cracking of each element was determined (reduction in the initial stiffness). The stiffness of the second model for the calculation of natural vibrations was defined near the SD limit state. The periods were prolonged due to a significant reduction in the stiffness of the structure in this case. Figure 12 shows the natural vibration modes of both models. The second vibration shape does not fully match the shape in the Y direction obtained via measurement since the partition walls are not modeled in the numerical model. In addition, the influence of the adjacent building is neglected. Modal participating mass ratios indicate that in the first natural periods in directions X and Y, the activation of the model mass is larger than 60%.
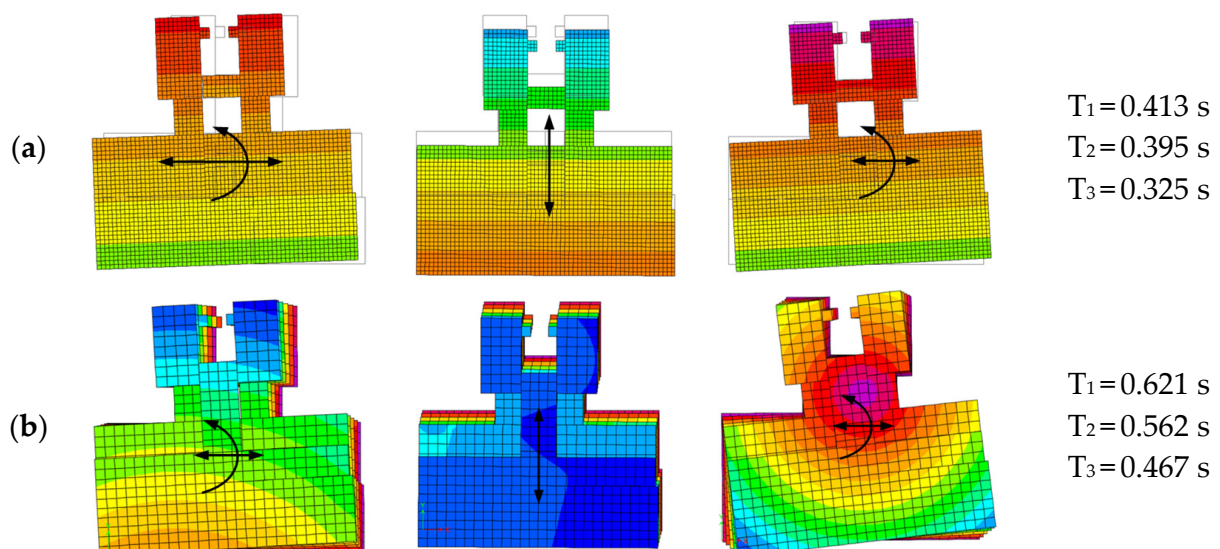

Figure 12. Natural mode shapes of the building: (**a**) adapted model for ambient vibrations, and (**b**) model of SD limit state.

5.4. Linear Analysis: Response Spectrum Method

A linear analysis using the response spectrum method was firstly considered. The design response spectrum, which is required in the CTRBS for seismic retrofitting at level 2, was used with a return period of 95 years. An eccentricity of 5% and behavior factor of 1.5 were considered in the analysis. Summarized results are presented below.

A check of the LD limit state is not prescribed in the CTRBS; therefore, this was performed according to the standard for new buildings. Figure 13a shows the displacement of the center of mass (CM) and maximum displacement for each story, while Figure 13b shows the inter-story drift. It should be noted that the elastic spectrum was considered in obtaining these results.
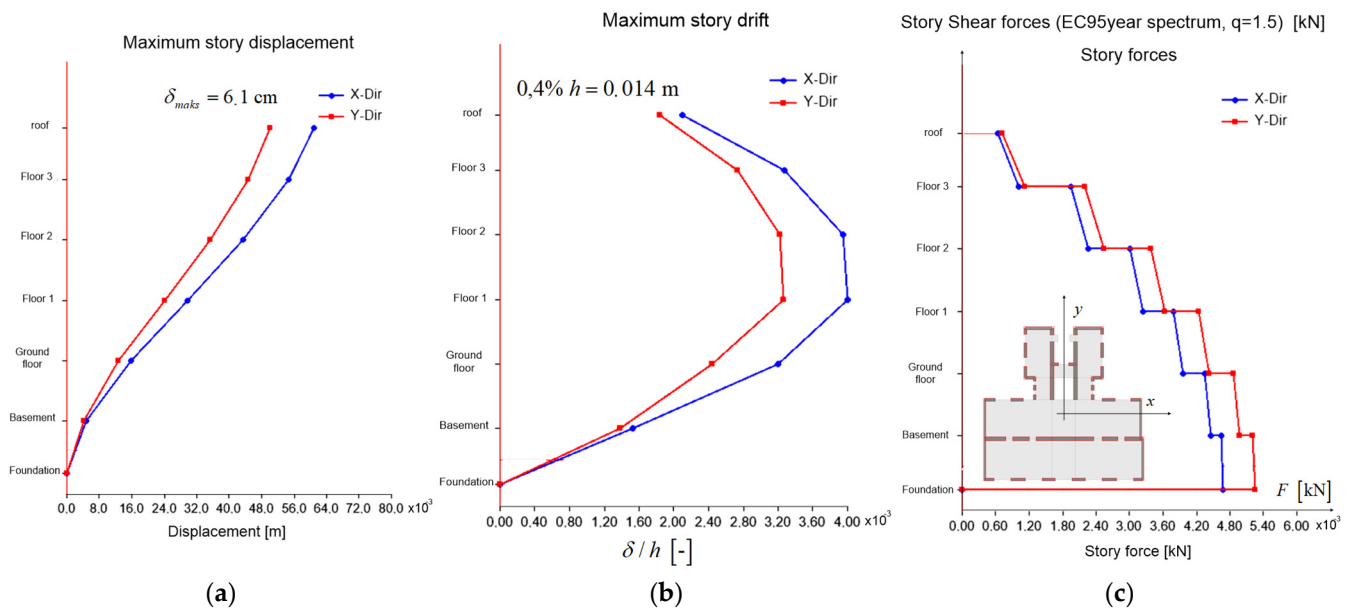

Figure 13. Response spectrum method results: (**a**) maximum story displacements. (**b**) maximum story inter-story drifts. (**c**) seismic lateral forces in the X and Y directions for a 95-year return period.

It can be observed that the maximum displacements are close to reaching the SD limit state and are up to 6 cm for the X direction and 5 cm for the Y direction in the attic. The maximum value of story drift for the X direction is approximately 0.004 ($\Delta/h = 0.4\%$), which is also the bounding value for the SD limit state for elements for which the shear failure mechanism is critical. This is not realistic since the model is linear–elastic, so displacement can be expected to be larger.

The distribution of story shear forces obtained using the design spectrum for a return period of 95 years is shown in Figure 13c. In the case of a 95-year return period, the value of the base shear (BS) coefficient is 15% for direction X and 16% for direction Y. The average shear stress in each story for a 95-year return period is between 0.14 and 0.16 MPa for the X and Y directions, with higher values corresponding to higher floors due to lesser thicknesses of walls. It is important to note that this method of calculating shear stress provides only a rough estimate and does not accurately represent the actual distribution. Since it is anticipated that the building will not meet the conditions of a 475-year return period earthquake, the analysis focuses on the effects of the 95-year earthquake ($a_g = 0.125$ g).

The following Figure 14 shows the results of wall seismic capacity analysis. It is evident that many elements exceed their shear force capacity by more than 200%, with some walls exceeding the load factor by more than 300%, which is well above the permissible values. In order to account for redistribution of forces due to nonlinear behavior of elements in this type of linear analysis, a redistribution of forces in load-bearing elements ranging from −25% to +33% was performed (according to the Eurocode). The condition for the application of the redistribution is that the resultant lateral force is unchanged (same intensity and position in each story). Figure 14b illustrates the outcomes of this redistribution, indicating that it has a beneficial impact on the utilization of the cross-section. It is important to highlight that a 25% reduction in internal forces in the critical element does not necessarily lead to a 25% decrease in utilization.
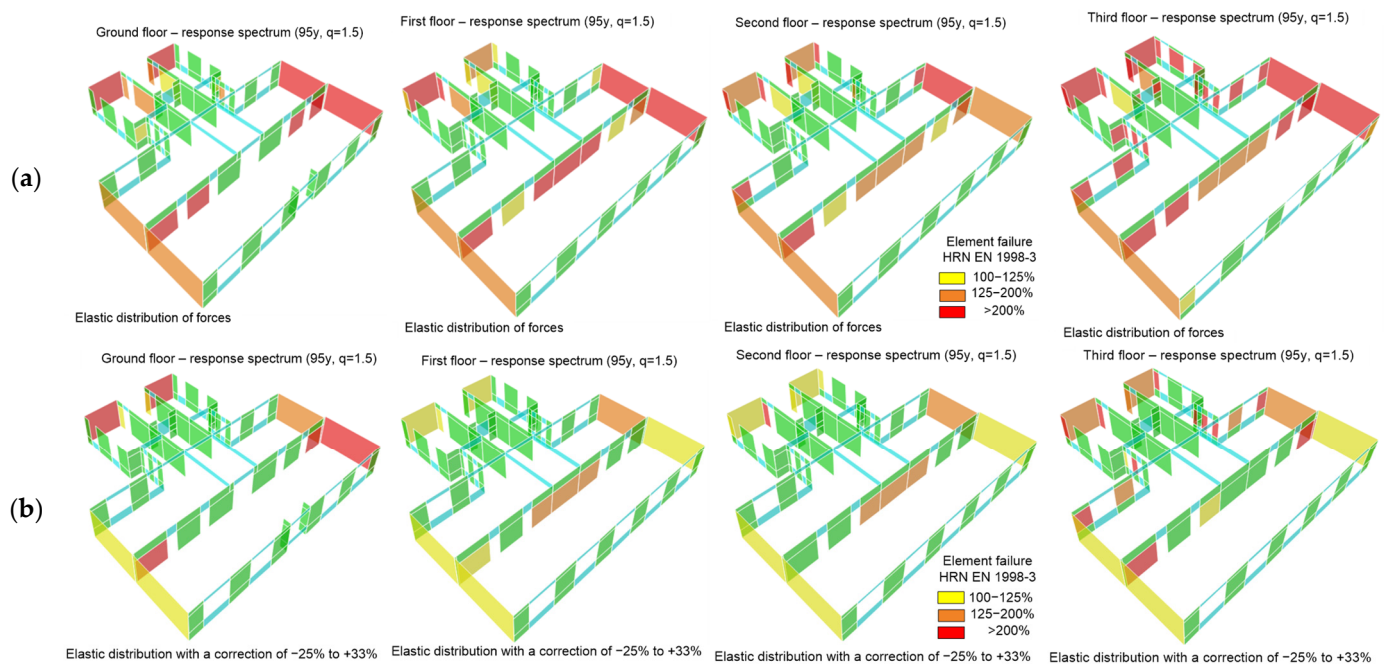
Figure 14. Summary of the wall shear capacity for seismic action with a 95-year return period (behavior factor 1.5) (**a**) without and (**b**) with redistribution performed.

In unreinforced masonry, high forces often lead to a significant reduction in the compressive area of the wall, which is crucial for its resistance to lateral loads. Therefore, a 25% reduction can significantly increase the compressive area and lead to even more of an increase in the element resistance. Besides the resistance of individual elements, it is important to consider the condition of the resultant force during redistribution of the 25% force from critical elements. If the structure has a high degree of static indeterminacy, this is not commonly a problem. However, if there are only a few walls in the floor plan or if there are individual walls that dominate the bearing of lateral loads (typically massive and/or long walls), satisfying the equality of the resultant force can be challenging. In this study, after conducting redistribution of forces in the model, a certain reduction in the utilization of the capacity of the elements was achieved; however, there were still elements exceeding the bearing capacity by over 200%.

In a further analysis, the response spectrum method was applied to determine the peak ground acceleration a_g at which the structure meets the required seismic capacity. For this purpose, design of the elements was carried out for the shear forces induced by the ground acceleration in the range of $a_g = 0.025$ g to $a_g = 0.125$ g. The allowable redistribution of internal forces was also considered in the calculations. Since this is a linear calculation, and some of the shear forces induced by the seismic lateral force changed linearly with the change in a_g, no new calculations needed to be performed. The results of the parametric calculation are shown in Figure 15. In the table, for each story of the building, the critical element utilization (calculated as the ratio of demand and capacity for lateral force) is given with respect to the peak ground acceleration in the soil category A. The same is shown in the diagram on the right, where the *x*-axis indicates the peak ground acceleration a_g value and the ordinate indicates the coefficient of capacity. The critical elements for each floor are marked in the floor plan and in the diagram.
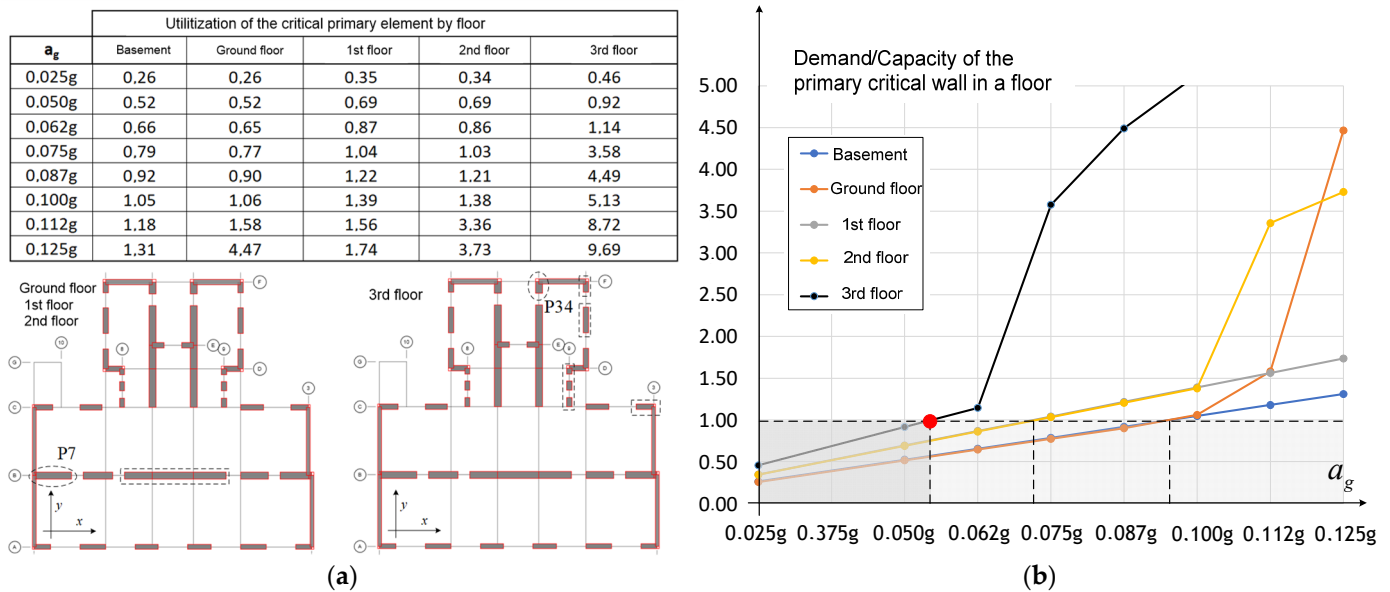
a_g	Utilitization of the critical primary element by floor				
	Basement	Ground floor	1st floor	2nd floor	3rd floor
0,025g	0,26	0,26	0,35	0,34	0,46
0,050g	0,52	0,52	0,69	0,69	0,92
0,062g	0,66	0,65	0,87	0,86	1,14
0,075g	0,79	0,77	1,04	1,03	3,58
0,087g	0,92	0,90	1,22	1,21	4,49
0,100g	1,05	1,06	1,39	1,38	5,13
0,112g	1,18	1,58	1,56	3,36	8,72
0,125g	1,31	4,47	1,74	3,73	9,69

Figure 15. Parametric analysis results for a_g. (**a**) critical element utilization by story. (**b**) demand/capacity of the primary critical wall in each story.

The SD limit state of the building was determined based on the critical elements on the 3rd floor, and was found to be only 43% of the demand for a_g = 0.125 g. The SD limit state of critical elements on the 1st and 2nd floors was then found to be 58%, while in the basement and on the ground floor, we found it to be 76% of the 95-year return period ground acceleration.

5.5. Nonlinear Static Method (Pushover)

The numerical model created in Etabs v.17 was extended to take into account the nonlinear behavior of the masonry elements by incorporating element capacity curves. A pushover analysis was conducted by applying various distributions of the lateral force and using the target displacement of the CM. Figure 16b shows the distribution patterns of acceleration along the height of the building. The load is applied in both the positive and negative directions of lateral force in the X and Y directions. Furthermore, the eccentricity value is regarded as being within a range of ±5% of the perpendicular plan dimension to the CM. A total of 72 calculations were carried out, of which only the most significant findings are showcased.

The load distribution that exhibits the most conservative behavior, known as the cantilever deformation line (cantilever), is represented by a dashed line. However, this load pattern is highly unlikely and is not considered relevant. Instead, the load distribution with a linear relationship between acceleration and height (linear) is considered to be the most detrimental. Similarly, but somewhat more favorably, the structure behaves in its load distribution according to the deformation line of the shear building, which follows a parabolic shape (shear).

The most favorable response and maximum load-bearing capacity of the structure were achieved when the lateral load was proportional to the inertial forces caused by the uniform acceleration of the masses. This acceleration pattern, along with the first mode of vibration, was decisive for the calculation using the pushover analysis. The results of the acceleration pattern corresponding to the fundamental mode in a particular direction (1st mode_X, 1st mode_Y) were nearly identical to the linear distribution.
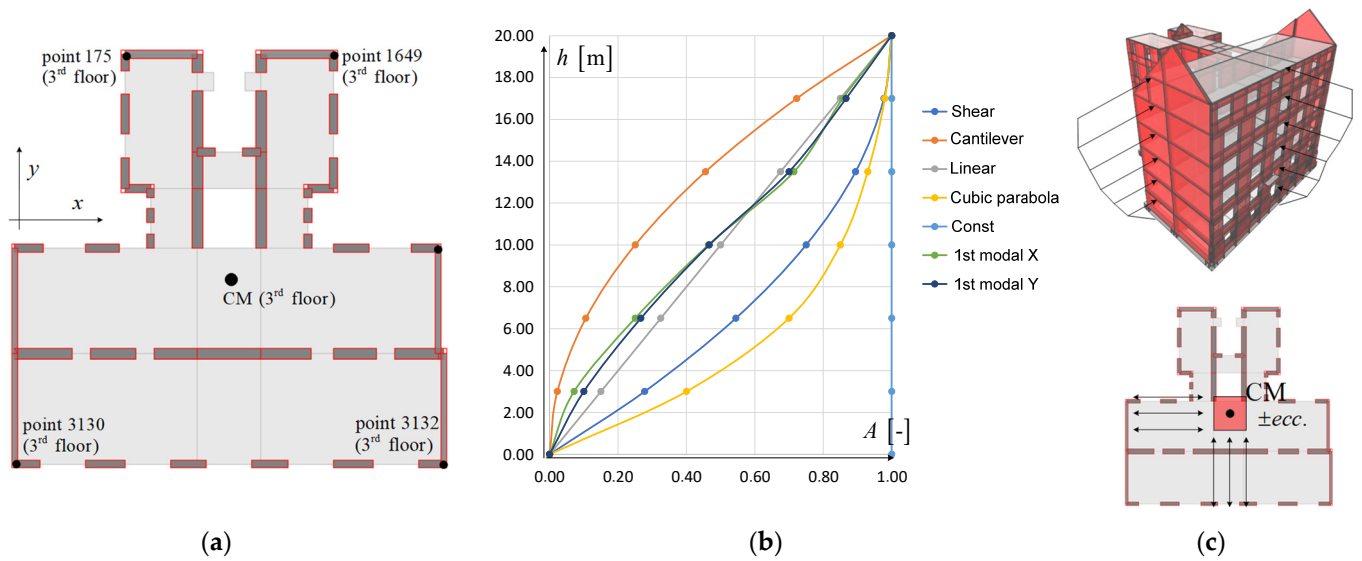
Figure 16. (**a**) Characteristic points on the 3rd floor; (**b**) distribution pattern of acceleration; (**c**) eccentricity of lateral force.

5.6. Building Capacity Curves for X Direction

Figure 17a illustrates the most important structural capacity curves for the positive direction X obtained using the load pattern of the lateral force method (red curves X/Y EFn) and the linear distribution (blue curves X/Y lin). The number in front of the marking indicates different directions and values of eccentricity. For a qualitative representation of the failure mechanism and the behavior of critical structural elements, key points on the curve are annotated to indicate structural element damage.
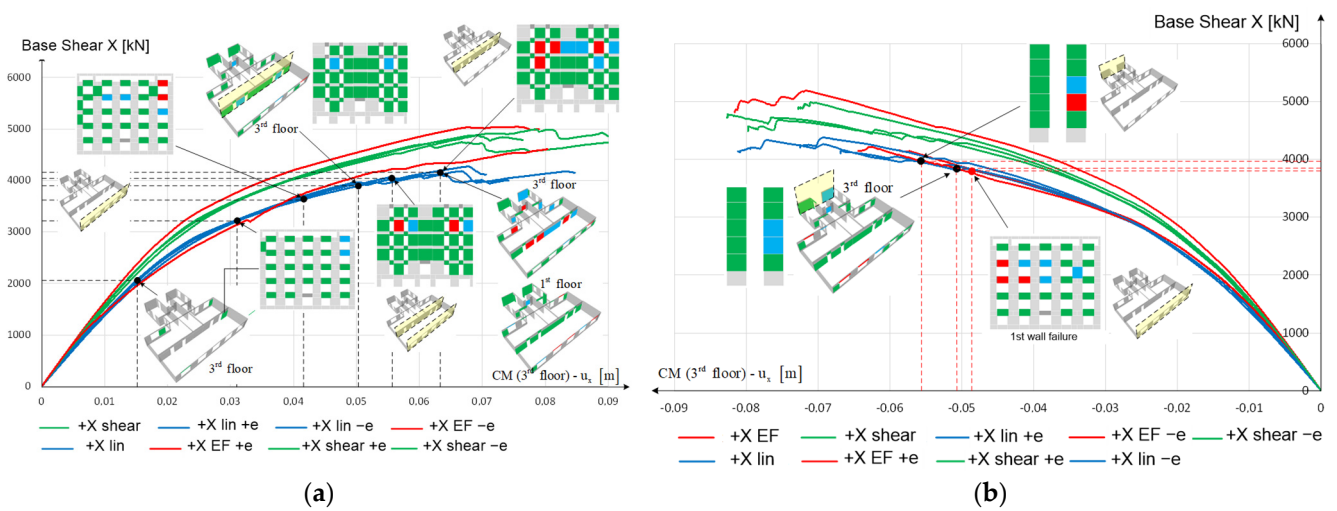
Figure 17. Relevant capacity curves of the building: (**a**) in the +X direction. (**b**) in the −X direction.

At a base shear value of approximately 2000 kN (base shear factor—BS = 6.2%) and a displacement of the CM on the 3rd floor of 1.5 cm, several structural elements reached a state of limited damage, resulting in a decrease in stiffness, as observed on the pushover curve. As the base shear increased, cracks opened, the stiffness of the building decreased, and damage occurred of several elements. The damage began on the 3rd floor of the building, where the load-bearing elements reached their yielding point. Nonetheless, these masonry structural elements have the ability to deform beyond their yielding point while retaining their load-bearing capacity. Therefore, an adequate approximation of the

pushover curves for individual elements is crucial for a high-quality analysis of the building pushover curve.

The first failure of a structural element occurred at a base shear force value of 3200 kN (B.S. = 10%) and a displacement of the CM on the 3rd floor of 3.1 cm. Several spandrels were observed to be in the SD limit state at this point. The next significant point was the failure of the spandrels on the street façade of the building at a base shear value of 3700 kN and a displacement of the CM on the 3rd floor of 4.2 cm. At this point, all the piers were still in a state of limited damage. It should be emphasized that these were "weak" spandrels, which are typical for masonry buildings in Zagreb.

The first pier failure occurred at a lateral force value of 4000 kN (B.S. = 12.5%) and a CM displacement of the 3rd floor of 5.1 cm. These were the piers on the 3rd floor in the central longitudinal axis of the building that reached the drift capacity, meaning localized failure of the floor structure could occur. It can be assumed that, at this point, the building was in a state of near collapse and had the highest degree of damage. Global failure occurred at a lateral force value of 4200 kN (B.S. = 13%) and a displacement of the 3rd floor CM of 6.3 cm. It should be noted that the walls of the basement, ground floor, and 1st floor were not critical for a positive direction of lateral force in the X direction.

The capacity curves for the negative X direction of the lateral load are depicted in Figure 17b. Similar to the previous case, the spandrels were the first to reach the SD limit state and so could be considered critical. In this scenario, the failure mechanism of the load-bearing system was initiated with the failure of the western courtyard wall on the 1st and 2nd floors. These walls reached the SD limit state at a lateral force of 3900 kN and a CM displacement of the 3rd floor of 5.1 cm, and their failure occurred when the displacement reached 5.6 cm. These piers were relatively rigid and located far from the CM, exposing them to significant shear forces caused by torsional effects resulting from the asymmetry and eccentricity of the load.

5.7. Building Capacity Curves for Y Direction

Capacity curves for the positive Y direction of lateral force are shown in Figure 18a. It is evident from the figure that some structural elements experienced an LD state when the base shear reached 2600 kN (B.S. = 8.1%) and the displacement of the 3rd floor CM was 1.6 cm. Primarily, these elements were located on the 3rd floor.
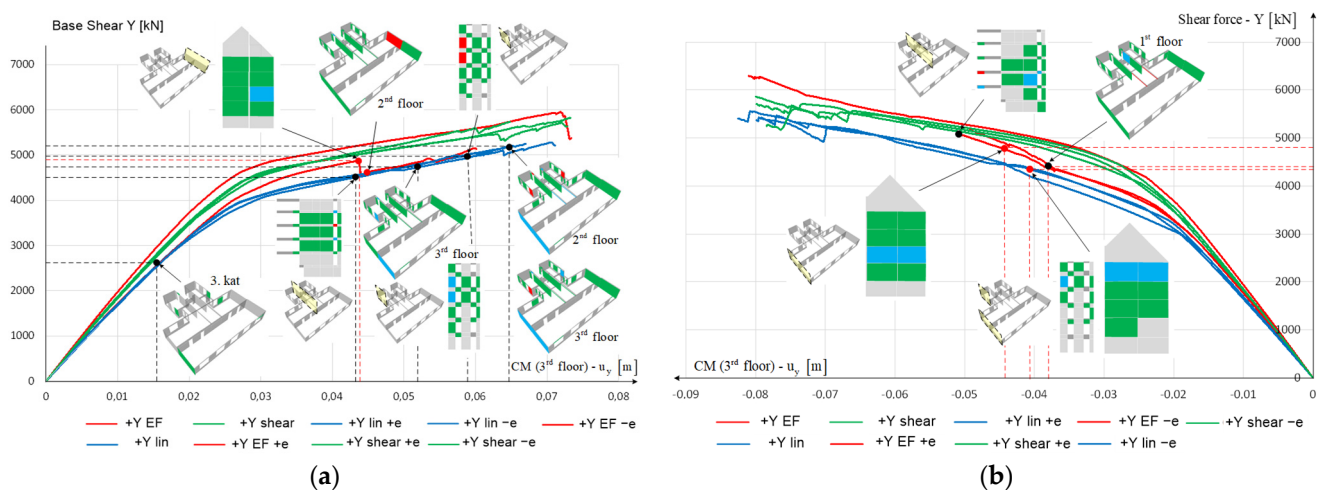

Figure 18. Relevant capacity curves of the building: (**a**) in the +Y direction. (**b**) in the −Y direction.

Just like the previous load case, applying the load in the Y direction also led to a consistent occurrence of exceeding the limit state for spandrels in terms of the SD. The spandrels that were critical and had limited rotation capacity were located at the edge of the central transverse wall along the staircase towards the west side of the building. The structural piers first exhibited failure when subjected to a lateral force of 4500 kN

(B.S. = 14%) and a displacement of 4.3 cm at the 3rd floor CM. The piers located on the north side of the building's north gable wall were the primary components that initially reached the SD limit state. This included the piers on the 1st floor, followed by the capacity of the piers on the 2nd floor being exceeded. Depending on the eccentricity of the load, the outermost south walls could also be regarded as critical components due to the building's symmetry in this direction. An interesting observation made of the capacity curve was a sudden significant drop (red curve) caused by the failure of the piers of the north gable wall. Despite the failure of several piers, the total lateral force continued to increase as the load increased. The walls of the courtyard façade on the 2nd and 3rd floors were the next elements where the SD limit state was exceeded in the transverse direction. As for the X direction, the building experienced critical pier failures primarily on its upper levels. Although the SD limit state was reached in several elements, the structure still maintained load-bearing capacity and ductility, preventing the building from collapsing. The ultimate displacement of the 3rd floor CM during global building collapse was estimated to be around 6.0 cm. The basement and ground floor walls were not considered critical for action in the positive Y direction.

The capacity curves for the lateral load in the negative Y direction (Figure 18b) indicate that the critical components were the spandrels, which reached the SD limit state first. In addition to the south gable wall, the staircase wall in the courtyard on the first floor of the building was also identified as critical for this load direction. In addition, it is important to note that the load-bearing capacity of reinforced concrete beams in the axes of the staircase was exceeded.

The failure mechanism of the vertical load-bearing system started when the piers in the south gable wall on the 3rd floor or in the western part were affected by the damaged piers in the staircase wall on the 1st floor of the building. These piers reached an SD limit state when subjected to a lateral force of about 4300 kN and a displacement of the 3rd floor CM of 3.9 cm.

Figure 19 presents a diagram showcasing the cumulative count of elements that reached the significant damage limit state. The diagram overlaps with the most important bearing capacity curve for the X direction. An area where the spandrels begin to enter a state of SD (highlighted in green) can be observed. It can be seen that in this area, a large number of spandrels, depending on the load case, enter a state of SD, and for critical cases already analyzed, the number is 38. After that, at a displacement of CM of about 5.1 cm, the critical pier enters a state of SD (red area), and soon after that, the critical pier also fails (near the red area).

5.8. Calculation of Capacity and Demand of the Building

The bearing capacity and building deformation requirement were also determined, which was achieved by reducing the system to an equivalent single-degree-of-freedom system (SDOF). The procedure was performed using the N2 method [49,50].

For each of the 72 load cases, a bearing capacity curve was obtained and verification for the peak ground acceleration was performed. Relevant curves and important parameters are laid out in the following text and figures.

Figure 20a,d show idealized bearing capacity curves of an equivalent SDOF system for a PGA of 0.125 g (r.p. 95 years—level 2) and for linear load distribution without eccentricity. The system's deformation capacity in both directions is higher than required. The maximum PGA value that would satisfy the demand in this case of load distribution is approximately 0.17 g for the X direction and 0.16 g for the Y direction. It should be noted that this load case is not paramount but is presented only to illustrate the main parameters and coefficients.
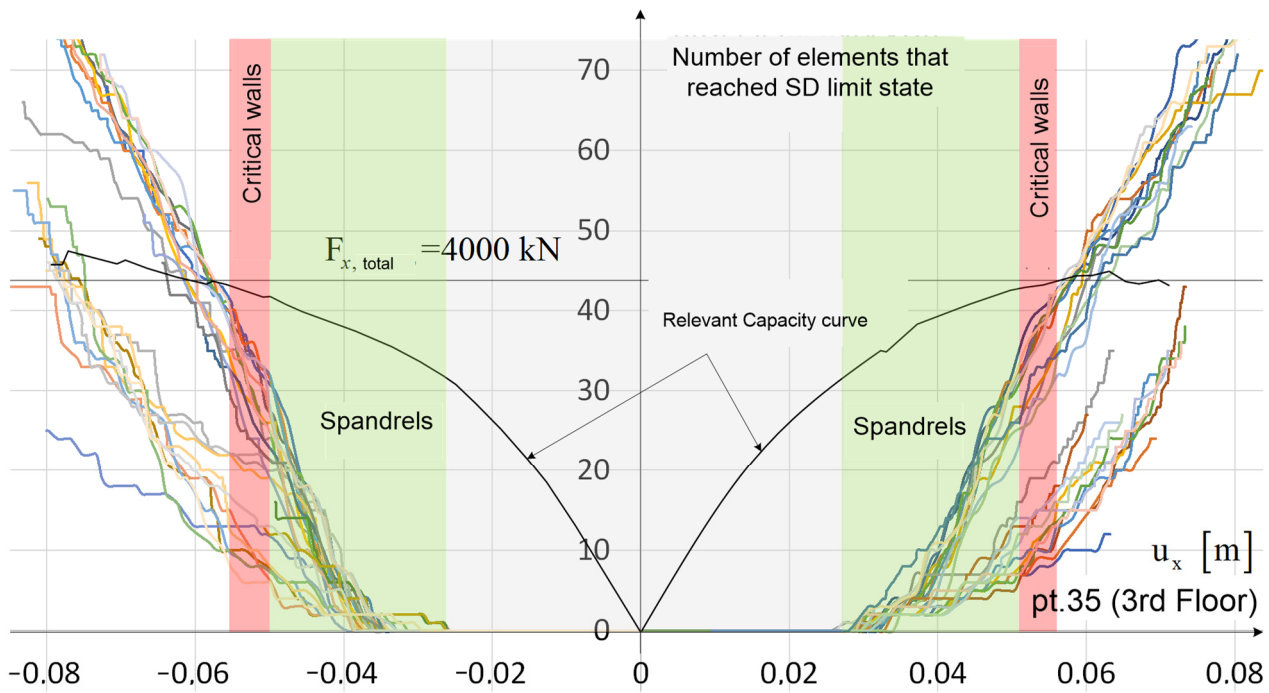
Figure 19. Number of elements that have reached the limit state SD as a function of the control point displacement.
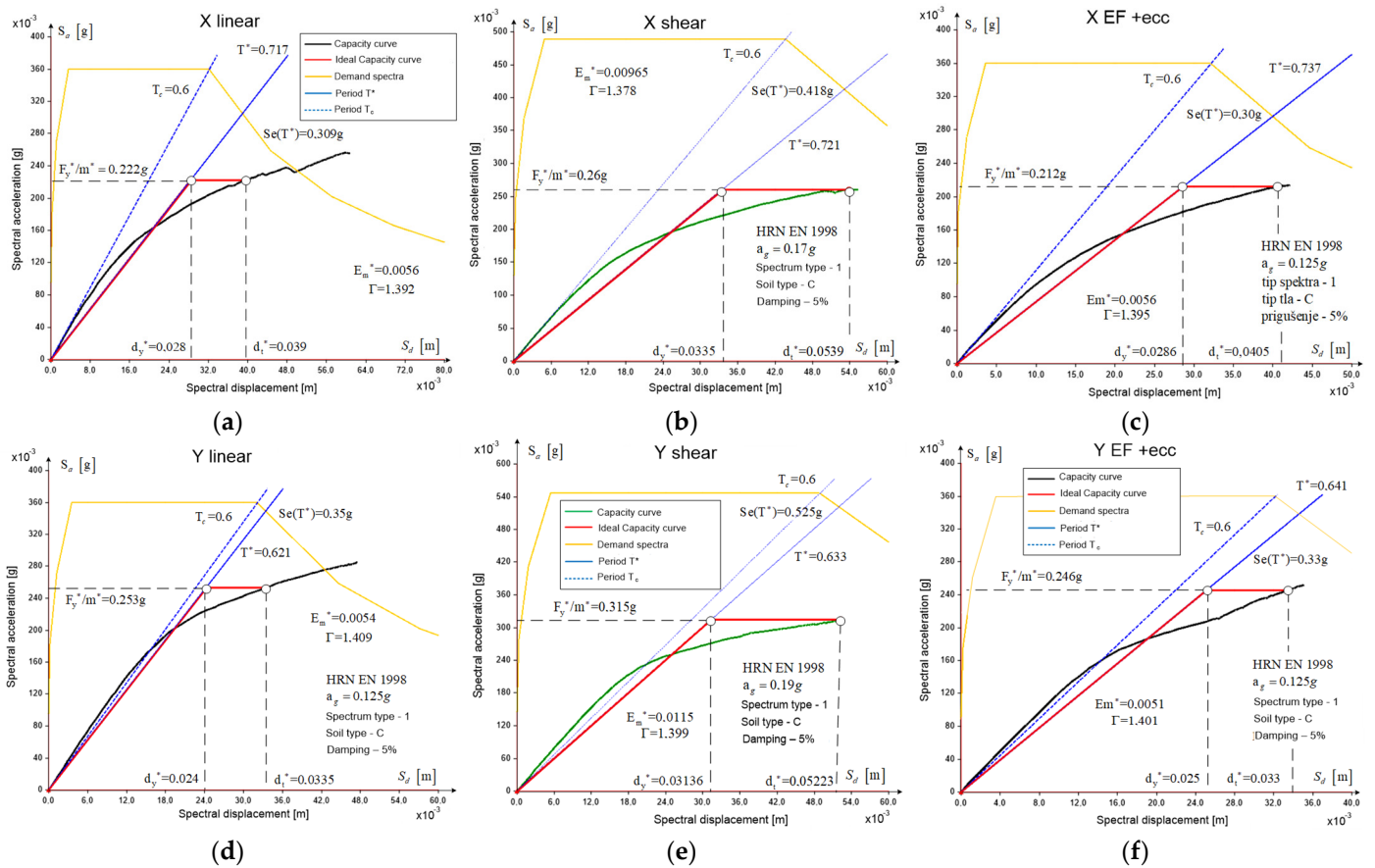

Figure 20. Relevant capacity curves of the building: linear load distribution directions X (**a**) and Y (**d**). shear load distribution directions X (**b**) and Y (**e**). lateral load method distribution directions X (**c**) and Y (**f**).

Similarly, Figure 20b,e show an idealized load capacity curve of an equivalent SDOF system for a PGA with 0.17 g in the X direction and 0.19 g in the Y direction for shear load distribution without eccentricity, as well as the load distribution during deformation of the shear building (parabola) also without eccentricity. It can be seen that for both distributions, the building has a similar deformation capacity that satisfies the ground acceleration requirement on the bedrock, of 0.17 g and 0.19 g, respectively, which is approximately equivalent to the earthquake return period of 225 years.

The capacity curves previously observed were for lateral force without eccentricity applied. When eccentricity is considered, the building capacity decreases considerably, as shown in the following illustration.

Figure 20c,f show the idealized capacity curve of an equivalent system for a ground acceleration on the base rock of 0.125 g for the X and Y directions and for a distribution of load over the height of the building using the lateral force method with a 5% eccentricity of the building width. The system deformation capacity can be concluded to be approximately equal to the required capacity. The maximum ground acceleration on the bedrock that fulfils the displacement requirement is close to 0.125 g, and this load case is critical. The system deformation capacity can be concluded to be close to the requirements, and we can surmise that there are no load-bearing reserves for horizontal actions.

5.9. Out-of-Plane Mechanisms (OOPs)

This kind of building typology has a high seismic vulnerability to out-of-plane failure of walls, i.e., partial mechanisms that are initiated by perpendicular seismic actions. Poor connections of the roof and floor structures and lack of horizontal and vertical constraining elements, as well as relatively low vertical loading, significantly contribute to the development of a kinematic chain. Since a finite element model is unable to represent this kind of failure mode, it was accounted for through an adaptation of the linear kinematic method assuming the formation of SDOF rigid block local mechanisms. The mechanism activation coefficient α_0 was determined through the application of the virtual work method and by determining effective mass ratio e* of the equivalent SDOF system. The corresponding spectral acceleration that activates the mechanism is given by $\alpha_0^* = \alpha_0 g / F_C e^*$, where Fc is the confidence factor equal to 1.35 for the rigid block assumption. For the subject building, local mechanisms selected for the OOP analysis are shown in Figures 21a and 22a. The first wall (wall_1) is the south gable wall, selected due to its slenderness and because on the portion of the gable, it has no connection with perpendicular elements. The other is the west courtyard wall of the annex (wall_2), selected because of presence of the near and large number of openings on the side walls and, similarly to the gable wall, because it is loaded only by its own weight (timber joists oriented parallel to the wall) and because prior global analysis showed that this wall could be significantly damaged by seismic actions. The main presumption for this mechanism is the failure of spandrels on the side walls.

For these two walls shown in Figure 21a, the position of the line hinge was considered to be a variable parameter. The results for the activation coefficient and corresponding spectral acceleration are given in Figure 21b,c. As the position of the line hinge increased over the height of the building, the volume of each block decreased and, as a consequence, the activation factor increased, manifesting the ratio of the thickness and height, i.e., elements with higher slenderness had a lower activation factor.

In addition, for the type of mechanism that considers the formation of an internal line hinge and the formation of a kinematic chain, two cases of façade walls were considered. It is worth noting that for these cases, a relatively good connection between floor structures and walls was assumed. The vertical position of the inner line hinge is assumed to be a variable parameter. For wall_3, it was assumed to form over the height of the pier and, for wall_4, it was assumed to form between the openings of the lower and upper floors. The results in Figure 22 show that the one-story mechanism (wall_3) had a high activation requirement regardless of the position of the internal line hinge formation. However, if the geometry of the local mechanism included two stories (wall_4), the activation coefficient

decreased considerably. Moreover, in this case, the sudden drop in the activation coefficient and spectral acceleration observed for the formation of the internal hinges at 13.2 m was a consequence of the change in wall thickness from 45 cm (lower story) to 30 cm (upper story), which was taken into account in the numerical calculation.
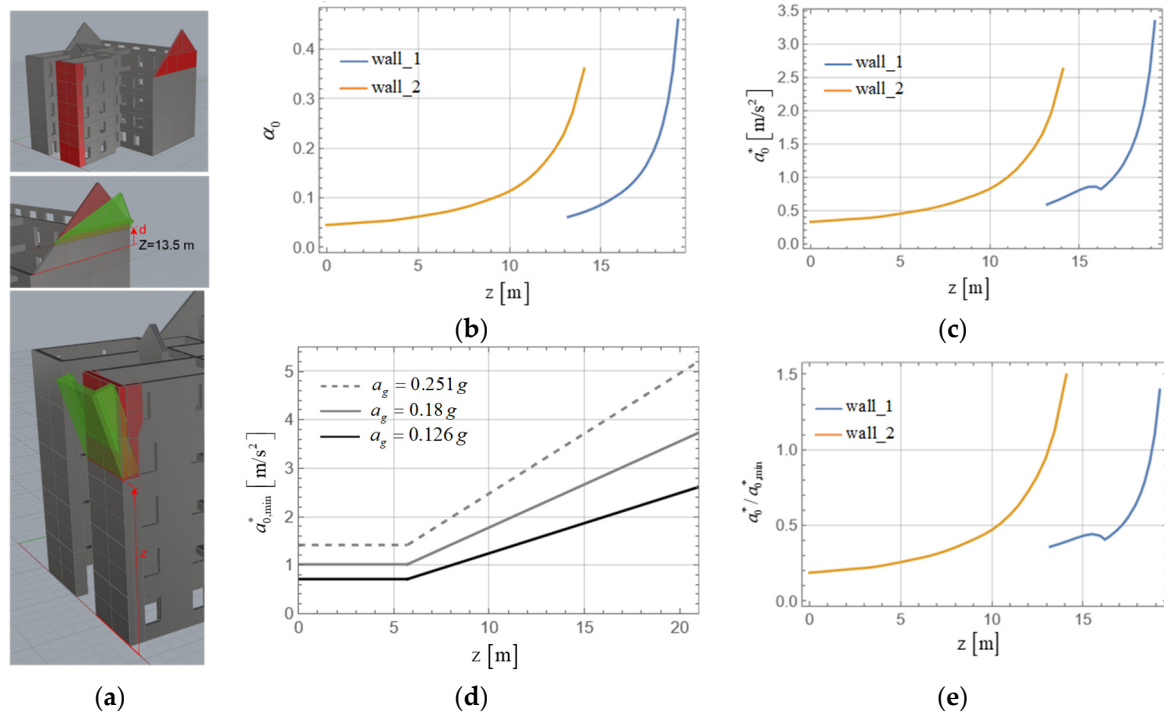

Figure 21. (**a**) Solid model of the case study building and selected overturning local mechanisms in Rhinocheros; (**b**) activation factor; (**c**) spectral acceleration that activates mechanism; (**d**) minimum demanded value for the spectral acceleration over the building height; and (**e**) safety factor value for the 95-year return period of seismic action.

In order to compare this to seismic action, the demand $a^*_{0,min} = max\left(a_g \frac{S}{q}; S_e(T_1)\Gamma_1 \frac{z}{H} q\right)$ was used, where the participation factor of the fundamental mode approximated by the number of stories is Γ_1, z is the height of the formation of the line hinge, H is building height, and q is a factor with the value 2. The corresponding minimum values are plotted for different return periods in Figure 21d. When comparing demand values with those obtained in the analysis, it was evident that for the return periods of 475 and 225 years, it does not satisfy requirements for all considered mechanisms except for wall_3. However, it should be mentioned that the formation of the line hinge of wall 2 below z = 10 m is unlikely because this mechanism assumes the formation of cracks on all spandrels of the orthogonal wall that will contribute to the separation of the considered wall. Furthermore, for the 95-year return period, the activation demand was satisfied in the case of a line hinge forming above the height of 13 m for the west courtyard wall (wall_2), and for gable (wall_1) above approximately z = 18.5 m. Nevertheless, it is worth mentioning that this analysis considered only the activation of the mechanism and not the eventual overturning of walls. Furthermore, this criterion is in most cases conservative, which is common of linear methods. Although the position of the line hinge of the presumed mechanisms shifted toward higher floors and the value of the activation acceleration increased, which was favorable, the walls of higher floors were still more prone to out-of-plane failure. Elements of the higher floors tended to be subjected to higher values of floor acceleration and generally had fewer connections, which constrained the mechanism to some extent, or like gable wall_1, they had no constraint at all. In the case of the two-story bending mechanism (wall_4), our investigation of the 95-year return period of seismic action returned an acceptable degree of

safety. However, the formation of this kind of mechanism is highly dependent on adequate constraint at the top of the mechanism.
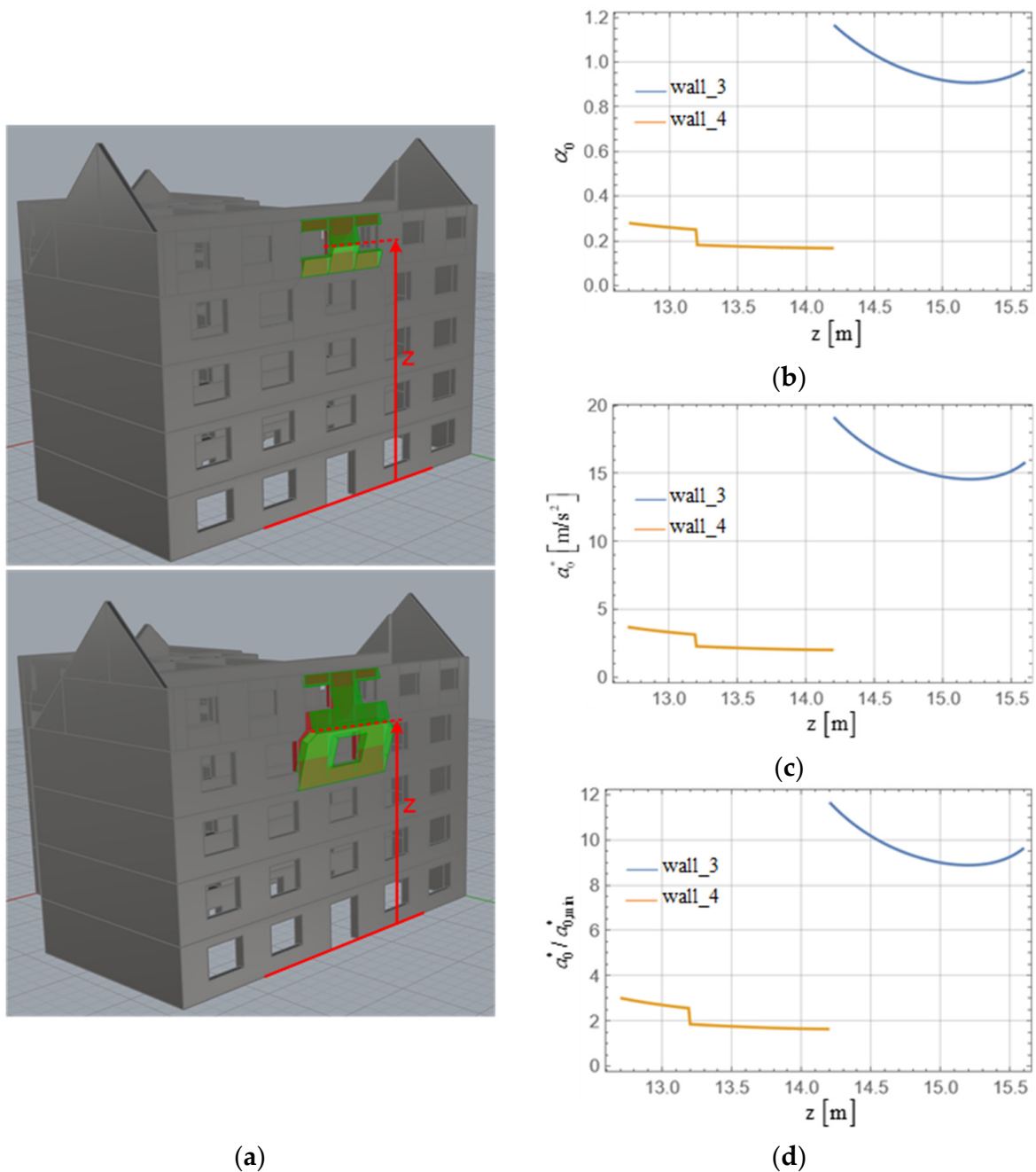

Figure 22. (**a**) Solid model of the one-story (wall_3) and two-story (wall_4) bending local mechanisms in Rhinocheros; (**b**) activation factor; (**c**) spectral acceleration that activates mechanism; and (**d**) safety factor value for the 95-year return period of seismic action.

6. Discussion

The main results of our analysis will be presented and a critical review of certain methods will be given in this section. Some ambiguities and problems arising from the application of simpler methods will be pointed out and the reasons will be explained.

Our analysis using the response spectrum method, which is commonly used for the design of new structures, resulted in a base shear force value of 15% of the weight for the X direction and 16% of the weight for the Y direction (with an importance factor of 1.0 and a

behavior factor of 1.5) for a return period of 95 years. Such a level of lateral forces resulted in significant local exceedance of the load-bearing capacity, even with the redistribution of internal forces. In our analysis with linear methods, due to their shortcomings, stress concentrations occurred regularly, so it often happened that short and slender elements were considerably overloaded. Such cases should be well analyzed because, strictly speaking, the resistance of a building is determined by the resistance of the critical primary elements. This requires professional engineering judgment and experience in analyzing the condition of existing buildings, as well as experience in numerical modeling, since there are often stress concentrations and unrealistically large internal forces in the elements due to inadequate discretization in the model and poor conditionality of the model. Therefore, it is important to consider which element failures affect structural stability and the capacity of surrounding load-bearing elements, and how much the load-bearing capacity is exceeded. If it is found that the force exceedance is relatively small and there are adjacent walls capable of resisting forces after the failure of the critical element, this type of isolated element can be ignored with caution. Therefore, it is very important to take into account the main disadvantage of linear calculations, namely that the distribution of forces is decided according to the stiffness that in reality changes during the dynamic response, and that ductility is not taken into account. Finally, the SD limit state of the building is determined by the critical elements on the third floor, which in this study, was only 43% of the demand for $a_g = 0.125$ g. The SD limit state of critical elements on the first and second floors occurred at 58%, while in the basement and on the ground floor, it was at 76% of the ground acceleration for a return period of 95 years.

An analysis of the building seismic performance using a nonlinear pushover method was carried out. Linear lateral force distribution proved to be the most relevant. All analyses showed a regular occurrence of exceeding the SD limit state of spandrels firstly. However, it is worth noting that the load capacity curves for spandrels have not been sufficiently studied and are often very conservative. Although failure of several spandrels will not cause partial structural collapse, especially if rigid or partially rigid diaphragms are ensured, they should be strengthened. Otherwise, the failure of the spandrels can lead to partial failure of the floor structures. The assumption is that the spandrels are secondary elements that do not compromise the overall stability of the structure. In the +X direction, the first pier failure occurred at the third floor, and it is very common for pier failures to occur at the higher floors of a building as a result of a low axial force that significantly reduces the load-bearing capacity of the elements. It is also worth mentioning that this type of building is constructed with a reduction in wall thickness at higher floors. Therefore, special attention should be paid to the higher floors of the building. Meanwhile, the −X direction showed that the failure mechanism was initiated by the damage of the piers at the first and second floors of the western courtyard wall, as a consequence of torsional effects caused by the asymmetry of the building plan and the eccentricity of the lateral force, but also by the low vertical load and the relatively high stiffness of these elements. The pushover analysis for the Y direction showed that, in addition to the spandrel failure already mentioned, the piers on the first and third floors of outermost south wall and the staircase wall were critical. Limit state control is carried out at the level of the whole structure and at the level of the element. If an element fails before the global load-bearing reserves are utilized, that element should be strengthened to ensure sufficient deformation capacity. Depending on the importance of the element for structural stability, it is possible to declare this element as secondary, which allows for an increase in the deformation capacity by up to 0.6% of the wall height. If we want to exploit the global load capacity reserves according to the load capacity curve of the building, intervention and strengthening of the critical elements in the higher floors of the building need to be ensured.

Relevant analyses were also conducted in comparison with the load-bearing capacity and building deformation requirement, which were achieved by reducing the system to an SDOF equivalent system carried out according to the N2 method. Only comparisons for a 95-year return period of seismic action were considered since it is the mandatory

minimum according to CTRBS. The cases of load distribution without eccentricity showed that in both directions, the building had same load-bearing reserves, and the maximum PGA ranged from 0.17 g to 0.19 g, approximately corresponding to the 225-year return period of seismic action and, therefore, almost sufficing to meet the requirement of Level 3 of CTRBS. However, when the eccentricity of the lateral force was taken into account, the PGA dropped to approximately 0.125 g, scarcely satisfying the CTRBS requirement for Level 2 of seismic resistance.

The possibility of activation of out-of-plane failure was also considered when performing a parametric analysis of the local mechanisms using the linear kinematic analysis method. The analysis carried out for the west courtyard wall showed the possible activation of the mechanism if the linear hinge formed below the third floor level when considering seismic action for a 95-year return period. By taking into account the damage patterns identified by the pushover analysis on the structural elements, especially on the piers and spandrels on the side walls, the possibility of the linear hinge formation and the activation of the mechanism between the first and third levels was found to be probable. Therefore, it is extremely important to draw special attention to strengthening connections, especially in the area of the lintels and parapets on the side walls. In addition, our analysis of the gable wall showed that it can be particularly critical for out-of-plane failure because it is partially cantilevered. It has low vertical loading (only self-weight), which has a stabilizing effect, and insufficient connections with perpendicular elements. While in the case of the west wall, the initiation of the overturning process depends on the damage of the joints, for this wall, it is very likely even with a very low intensity of seismic action. Finally, the numerical analysis of the cases in which a kinematic two-body chain was formed showed that this mechanism should be the preferred one, but it requires that adequate connections with the floor structures are provided on each floor.

7. Conclusions

In this paper, a seismic assessment of a typical unreinforced masonry building in Zagreb was performed through different numerical modeling approaches and analysis methods, including response spectrum, pushover, and out-of-plane wall failure analyses. After a detailed inspection of the building, experimental investigations, and numerical analyses of the building's seismic performance, the following conclusions and recommendations can be offered:

- The building was severely damaged in a relatively moderate earthquake, which proves its significant seismic vulnerability and the need for further research on this type of building.
- When measuring the ambient vibrations before and after the earthquake, a change in natural frequencies of about 10% was observed, which proved that some of the load-bearing walls of the building are damaged and that they are in a cracking condition.
- Analysis using the response spectrum method provided significantly conservative values of the load-bearing capacity. Also, the mechanism of structural failure could not be reliably determined. The main reason for this was that the distribution of forces was carried out exclusively according to the stiffness of the elements, and the behavior factor was constant (equal to 1.5) for the entire building.
- According to the response spectrum method, the limit state of the SD was determined by the critical primary elements on the third floor, which was only 43% of the requirement for $a_g = 0.125$ g (95-year return period earthquake).
- When using the pushover method with various shapes and directions of loading, it was regularly found that the spandrels were the first elements to be damaged and later fail. Moreover, the appearance of wall damage was mainly observed on the higher floors of the building, which was the result of the low axial force and the absence of a rigid diaphragm.
- For the direction of action X, the influence of eccentricity and torsion on the overall load-bearing capacity of the building was characteristic. The failure mechanism was

initiated by damage to the first and second floors of the western courtyard wall, which was a consequence of the torsional effects caused by the asymmetry of the building's floor plan and the eccentricity of the lateral force. The analysis showed that the influence of eccentricity was significant for certain elements.

- When implementing the N2 method, we found that the structure met the requirement for peak ground acceleration of approximately 0.125 g (95-year return period earthquake), which corresponds to the required level of seismic resistance according to CTRBS.
- Out-of-plane analysis pointed to the key problem of this type of building. The analysis of the gable wall and the west wall showed that it was a critical failure mechanism. Similar patterns of damage and failure were also shown in the earthquake. Even for small earthquake intensities, it is likely that there will be out-of-plane damage to the walls due to the absence of floor panels that properly connect the walls in the floor plan.
- The main problem of this typology can be highlighted, which is the lack of rigid transverse walls of the building to connect the main load-bearing longitudinal walls. The gable walls are long and without openings, but they are relatively thin and are not connected to the floor structures, and they are quite distant from each other. Apart from those, there are staircase walls in the transverse direction, but they generally have many openings and do not significantly contribute to the lateral load transfer.
- Finally, an unfavorable circumstance is the partially divided floor plan of the building, which forms two units (the eastern unit facing the street and the western unit facing the courtyard). The location of the staircase at the intersection of these two units creates the risk that, in the event of an earthquake, these two units will respond separately. Their separation could have significant consequences for the building.

In this paper, the influence of the position of the building in the building aggregate was not analyzed, though it certainly has an influence on the load-bearing capacity of the building. This effect deserves to be the subject of special research, which is currently being carried out.

References

1. Uroš, M.; Todorić, M.; Crnogorac, M.; Atalić, J.; Šavor Novak, M.; Lakušić, S. *Potresno Inženjerstvo—Obnova Zidanih Zgrada*; University of Zagreb, Faculty of Civil Engineering: Zagreb, Croatia, 2021.
2. So, E.; Babić, A.; Majetic, H.; Putrino, V.; Verrucci, E.; Contreras Mojica, D.; Rossetto, T.; Wilkinson, S.; Keogh, C.; D'Ayala, D. *The Zagreb Earthquake of 22 March 2020*; EEFIT: London, UK, 2020.
3. Miranda, E.; Brzev, S.; Bijelic, N.; Arbanas, Ž.; Bartolac, M.; Jagodnik, V.; Lazarević, D.; Mihalić Arbanas, S.; Zlatović, S.; Acosta, A.; et al. *Petrinja, Croatia December 29, 2020, Mw 6.4 Earthquake Joint Reconnaissance Report (JRR)*; ETH: Zurich, Switzerland, 2021.

4. Šavor Novak, M.; Uroš, M.; Atalić, J.; Herak, M.; Demšić, M.; Baniček, M.; Lazarević, D.; Bijelić, N.; Crnogorac, M.; Todorić, M. Zagreb earthquake of 22 March 2020—Preliminary report on seismologic aspects and damage to buildings. *Građevinar* **2020**, *72*, 843–867. [CrossRef]

5. Atalić, J.; Uroš, M.; Šavor Novak, M.; Demšić, M.; Nastev, M. The Mw5.4 Zagreb (Croatia) earthquake of March 22, 2020: Impacts and response. *Bull. Earthq. Eng.* **2021**, *19*, 3461–3489. [CrossRef]

6. Available online: https://www.pmf.unizg.hr/geof/seizmoloska_sluzba/potresi_kod_petrinje?@=1m6dc#news_118053 (accessed on 5 May 2023).

7. Atalić, J.; Demšić, M.; Baniček, M.; Uroš, M.; Dasović, I.; Prevolnik, S.; Kadić, A.; Šavor Novak, M.; Nastev, M. The December 2020 magnitude (Mw) 6.4 Petrinja earthquake, Croatia: Seismological aspects, emergency response and impacts. *Bull. Earthq. Eng.* **2023**, *21*, 5767–5808. [CrossRef]

8. Atalić, J.; Šavor Novak, M.; Uroš, M. *Updated Risk Assessment of Natural Disasters in Republic of Croatia—Seismic Risk Assessment*; Faculty of Civil Engineering in collaboration with Ministry of Construction and Physical Planning and National Protection and Rescue Directorate: Zagreb, Croatia, 2018. (In Croatian)

9. Simović, V. Potresi na zagrebačkom području. *Građevinar* **2000**, *52*, 637–645.

10. Markušić, S.; Stanko, D.; Korbar, T.; Belić, N.; Penava, D.; Kordić, B. The Zagreb (Croatia) M5.5 Earthquake on 22 March 2020. *Geosciences* **2020**, *10*, 252. [CrossRef]

11. Crnogorac, M.; Todorić, M.; Uroš, M.; Atalić, J. *Emergency seismic reconstruction program—UPPO*; Faculty of Civil Engineering, University of Zagreb: Zagreb, Croatia; Croatian Association of Civil Engineers: Zagreb, Croatia, 2020. (In Croatian)

12. Uroš, M.; Šavor Novak, M.; Atalić, J.; Sigmund, Z.; Baniček, M.; Demšić, M.; Hak, S. Post-earthquake damage assessment of buildings—Procedure for conducting building inspections. *J. Croat. Assoc. Civ. Eng.* **2021**, *72*, 1089–1115. [CrossRef]

13. Atalić, J.; Demšić, M.; Lazarević, D.; Uroš, M.; Baniček, M.; Todorić, M. *Report on the Assessment of the Existing Condition of the Zagreb University Building*; University of Zagreb: Zagreb, Croatia, 2021. (In Croatian)

14. Pinasco, S.; Cattari, S.; Lagomarsino, A.; Demšić, M.; Šavor Novak, M.; Uroš, M. Numerical investigation of the seismic response of an unreinforced masonry residential buildings hit by Zagreb earthquake in 2020. In Proceedings of the 2nd Croatian Conference on Earthquake Engineering 2023, Zagreb, Croatia, 22–24 March 2023. [CrossRef]

15. Moretić, A.; Chieffo, N.; Stepinac, M.; Lourenço, P.B. Vulnerability assessment of historical building aggregates in Zagreb: Implementation of a macroseismic approach. *Bull. Earthq. Eng.* **2022**, *21*, 2045–2065. [CrossRef]

16. Stepinac, M.; Lourenço, P.B.; Atalić, J.; Kišiček, T.; Uroš, M.; Baniček, M.; Šavor Novak, M. Damage classification of residential buildings in historical downtown after the ML5.5 earthquake in Zagreb, Croatia in 2020. *Int. J. Disaster Risk Reduct.* **2021**, *56*, 102140. [CrossRef]

17. Acito, M.; Buzzetti, M.; Cundari, G.A.; Milani, G. General methodological approach for the seismic assessment of masonry aggregates. *Structures* **2023**, *57*, 105177. [CrossRef]

18. Tomić, I.; Penna, A.; DeJong, M.; Butenweg, C.; Correia, A.A.; Candeias, P.X.; Senaldi, I.; Guerrini, G.; Malomo, D.; Wilding, B.; et al. Shake-table testing of a stone masonry building aggregate: Overview of blind prediction study. *Bull. Earthq. Eng.* **2023**. [CrossRef]

19. Ferreira, T.M.; Costa, A.A.; Costa, A. Analysis of the Out-Of-Plane Seismic Behavior of Unreinforced Masonry: A Literature Review. *Int. J. Arch. Heritage* **2014**, *9*, 949–972. [CrossRef]

20. D'altri, A.M.; Sarhosis, V.; Milani, G.; Rots, J.; Cattari, S.; Lagomarsino, S.; Sacco, E.; Tralli, A.; Castellazzi, G.; de Miranda, S. Modeling Strategies for the Computational Analysis of Unreinforced Masonry Structures: Review and Classification. *Arch. Comput. Methods Eng.* **2019**, *27*, 1153–1185. [CrossRef]

21. Betti, M.; Galano, L.; Vignoli, A. Comparative analysis on the seismic behaviour of unreinforced masonry buildings with flexible diaphragms. *Eng. Struct.* **2014**, *61*, 195–208. [CrossRef]

22. Ottonelli, D.; Manzini, C.F.; Marano, C.; Cordasco, E.A.; Cattari, S. A comparative study on a complex URM building: Part I—Sensitivity of the seismic response to different modelling options in the equivalent frame models. *Bull. Earthq. Eng.* **2021**, *20*, 2115–2158. [CrossRef]

23. Cattari, S.; Calderoni, B.; Caliò, I.; Camata, G.; de Miranda, S.; Magenes, G.; Milani, G.; Saetta, A. Nonlinear modeling of the seismic response of masonry structures: Critical review and open issues towards engineering practice. *Bull. Earthq. Eng.* **2021**, *20*, 1939–1997. [CrossRef]

24. Cattari, S.; Magenes, G. Benchmarking the software packages to model and assess the seismic response of unreinforced masonry existing buildings through nonlinear static analyses. *Bull. Earthq. Eng.* **2021**, *20*, 1901–1936. [CrossRef]

25. Lagomarsino, S.; Camilletti, D.; Cattari, S.; Marino, S. Seismic assessment of existing irregular masonry buildings by nonlinear static and dynamic analyses. In *Recent Advances in Earthquake Engineering in Europe: 16th European Conference on Earthquake Engineering, Thessaloniki, Greece, 18–21 June 2018*; Springer International Publishing: Cham, Switzerland, 2018; pp. 123–151. [CrossRef]

26. Tomić, I.; Vanin, F.; Beyer, K. Uncertainties in the Seismic Assessment of Historical Masonry Buildings. *Appl. Sci.* **2021**, *11*, 2280. [CrossRef]

27. Angiolilli, M.; Brunelli, A.; Cattari, S. Fragility curves of masonry buildings in aggregate accounting for local mechanisms and site effects. *Bull. Earthq. Eng.* **2023**, *21*, 2877–2919. [CrossRef]

28. Brunelli, A.; de Silva, F.; Cattari, S. Site effects and soil-foundation-structure interaction: Derivation of fragility curves and comparison with Codes-conforming approaches for a masonry school. *Soil Dyn. Earthq. Eng.* **2021**, *154*, 107125. [CrossRef]

29. D'Ayala, D.; Speranza, E. Definition of Collapse Mechanisms and Seismic Vulnerability of Historic Masonry Buildings. *Earthq. Spectra* **2003**, *19*, 479–509. [CrossRef]

30. *NIKER Project—Critical Review of Methodologies and Tools for Assessment of Failure Mechanisms and Interventions, Deliverable 3.3, WORKPACKAGE 3: Damage Based Selection of Technologies*; NIKER Project: Padova, Italy, 2010.

31. Ferreira, T.M.; Costa, A.A.; Arêde, A.; Gomes, A.; Costa, A. Experimental characterization of the out-of-plane performance of regular stone masonry walls, including test setups and axial load influence. *Bull. Earthq. Eng.* **2015**, *13*, 2667–2692. [CrossRef]

32. de Felice, G. Out-of-Plane Seismic Capacity of Masonry Depending on Wall Section Morphology. *Int. J. Arch. Heritage* **2011**, *5*, 466–482. [CrossRef]

33. Costa, A.A.; Arêde, A.; Costa, A.; Oliveira, C.S. Out-of-plane behaviour of existing stone masonry buildings: Experimental evaluation. *Bull. Earthq. Eng.* **2011**, *10*, 93–111. [CrossRef]

34. Costa, A.A.; Arêde, A.; Costa, A.C.; Penna, A.; Costa, A. Out-of-plane behaviour of a full scale stone masonry façade. Part 1: Specimen and ground motion selection. *Earthq. Eng. Struct. Dyn.* **2013**, *42*, 2081–2095. [CrossRef]

35. Costa, A.A.; Arêde, A.; Costa, A.C.; Penna, A.; Costa, A. Out-of-plane behaviour of a full scale stone masonry façade. Part 2: Shaking table tests. *Earthq. Eng Struct. Dyn.* **2013**, *42*, 2097–2111. [CrossRef]

36. Degli Abbati, S.; Rossi, M.; Lagomarsino, S. Out-of-plane experimental tests on masonry panels. In Proceedings of the 2nd European Conference on Earthquake Engineering and Seismology, Istanbul, Turkey, 25–29 August 2014.

37. Grillanda, N.; Valente, M.; Milani, G. ANUB-Aggregates: A fully automatic NURBS-based software for advanced local failure analyses of historical masonry aggregates. *Bull. Earthq. Eng.* **2020**, *18*, 3935–3961. [CrossRef]

38. Funari, M.F.; Mehrotra, A.; Lourenço, P.B. A Tool for the Rapid Seismic Assessment of Historic Masonry Structures Based on Limit Analysis Optimisation and Rocking Dynamics. *Appl. Sci.* **2021**, *11*, 942. [CrossRef]

39. Mercuri, M.; Pathirage, M.; Gregori, A.; Cusatis, G. Computational modeling of the out-of-plane behavior of unreinforced irregular masonry. *Eng. Struct.* **2020**, *223*, 111181. [CrossRef]

40. Aşıkoğlu, A.; Vasconcelos, G.; Lourenço, P.B.; Pantò, B. Pushover analysis of unreinforced irregular masonry buildings: Lessons from different modeling approaches. *Eng. Struct.* **2020**, *218*, 110830. [CrossRef]

41. Herak, M.; Allegretti, I.; Herak, D.; Ivančić, I.; Kuk, V.; Marić, K.; Markušić, S.; Sović, I. Republika Hrvatska, Karta potresnih Područja. 2011. Available online: http://seizkarta.gfz.hr (accessed on 5 May 2023).

42. Milutinovic, Z.; Trendafilovski, G. *An Advanced Approach to Earthquake risk Scenarios with Applications to Different European Towns—WP4: Vulnerability of Current Buildings*; RISK-EU; Bureau de Recherches Géologiques et Minières: Orleans, France, 2003; 110p.

43. Lagomarsino, S.; Giovinazzi, S. Macroseismic and mechanical models for the vulnerability and damage assessment of current buildings. *Bull. Earthq. Eng.* **2006**, *4*, 415–443. [CrossRef]

44. Grünthal, G. *European Macroseismic Scale 1998 (EMS-98)*; Cahiers du Centre Européen de Géodynamique et de Séismologie 15; Centre Européen de Géodynamique et de Séismologie: Luxembourg, 1998.

45. *HRN EN 1998-3*; Eurocode 8: Design of Structures for Earthquake Resistance—Part 3: Assessment and Retrofitting of Buildings. HZN: Zagreb, Croatia, 2011. (In Croatian)

46. *ASTM C1531-16*; Standard Test Methods for In Situ Measurement of Masonry Mortar Joint Shear Strength Index. ASTM: West Conshohocken, PA, USA, 2016.

47. CSI. *CSI Analysis Reference Manual for SAP2000, ETABS, SAFE and CSiBridge*; Computers and Structures Inc.: Berkeley, CA, USA, 2017.

48. *ASCE/SEI 41-13*; Seismic Rehabilitation of Existing Buildings. American Society of Civil Engineers: Reston, VA, USA, 2014; ISBN 9780784412855.

49. Fajfar, P.; Gašperšič, P. The N2 method for the seismic damage analysis of RC buildings. *Earthq. Eng. Struct. Dyn.* **1996**, *25*, 31–46. [CrossRef]

50. Fajfar, P. A nonlinear analysis method for performance-based seismic design. *Earthq. Spectra* **2000**, *16*, 573–592. [CrossRef]